GEOLOGIAN TUTKIMUSKESKUS
TMI
Espoo- Rovaniemi

10.6.2016 55/2016

Mineralogy and geochemistry of flake graphite occurrences in Joutsijärvi, Northern Finland

Thair Al-Ani and Olli Sarapää

GEOLOGIAN TUTKIMUSKESKUS • GEOLOGISKA FORSKNINGSCENTRALEN • GEOLOGICAL SURVEY OF FINLAND

PL/PB/P.O. Box 96
FI-02151 Espoo, Finland

PL/PB/P.O. Box 1237
FI-70211 Kuopio, Finland

PL/PB/P.O. Box 97
FI-67101 Kokkola, Finland

PL/PB/P.O. Box 77
FI-96101 Rovaniemi, Finland

Puh. 029 503 0000 • Tel. +358 29 503 0000 • www.gtk.fi • Y-tunnus / FO-nummer / Business ID: 0244680-7

GEOLOGIAN TUTKIMUSKESKUS
TMI
Espoo- Rovaniemi

10.6.2016 55/2016

GEOLOGICAL SURVEY OF FINLAND DOCUMENTATION PAGE

Date / Rec. no.

Authors Thair Al-Ani and Olli Sarapää	Type of report Archive report
	Commissioned by GTK

Title of report
Mineralogy and geochemistry of flake graphite occurrences in Joutsijärvi, Northern Finland

Abstract
This research report focuses on mineralogy and geochemistry of the graphite schist from the Joutsijärvi and Kemijärvi areas Northern Finland. The drill core samples were studied by using optical microscopy, scanning electron microscopy (SEM), X-ray diffraction (XRD) in combination with Siroquant software, X-ray fluorescence (XRF), and inductively coupled plasma mass spectrometry (ICP-MS). Graphite occurs as parallel orientation of flakes within graphite-sulphide-schist. Independently of mineralogical and textural studies graphite is characterized by its coarse flakes, fully ordered, high purity and crystallinity, which are required for applications in advanced technologies. The carbon shows medium to high median concentrations between 2% to 28%. Gangue minerals in the schists are quartz, plagioclase, K-feldspar, biotite and iron sulfide minerals.

XRD data indicate that all the studied graphite is structurally fully ordered (crystal1iesized), Lc (002) ranging from 485 to 684 Å), possess high degree of graphitization (DG value ranging from 108 to 205 A) and reflect crystallization at high temperature (520°C to 830°C).

The graphite schists were originally sediments rich in organic matter which was converted to graphite during metamorphism process. At the low grade regional metamorphism stage, the schistosity was developed in the rocks, and its heat and pressure were responsible for the formation of graphite and other metamorphic minerals as chlorite and biotite. On the basis of graphite flakes and mineral assemblages present in the studied rocks, it can be it can be inferred that those consisting of micro-graphite flakes (amorphous) are the result of low-grade metamorphism (chlorite zone) and those having well-developed flakes of graphite (flaky) are due to medium to high grade metamorphism (biotite-zone).

Keywords
Graphite, graphite, flake graphite, high-grade metamorphism, Kuusivaara, Joutsijärvi, Central Lapland , Finland

Geographical area Kuusivaara, Joutsijärvi, Central Lapland

Map sheet 3632, 3624

Report serial Archive report		Archive code	
Total pages 39p	Language English	Price	Confidentiality
Unit and section		Project code 50402-20048	
Signature/name		Signature/name	

Contents

Documentation page

1 INTRODUCTION

1.1 Graphite production and use

Graphite is considered as critical mineral by both in USA and the EU due to its rather low abundance in nature and because it is a strategic material for the manufacturing of electronic devices, lubricants, cathode for Li-ion batteries and use in nanotechnology. It is expected that the demand for graphite will increase approximately 4% in the coming years (Lazzeri and Barreiro 2014). In the industry, the biggest consumer of flake graphite is refractories industry, because flake graphite improves refractory products' resistance to heat and erosion.

In 2015 total world graphite production was 1.19 million tons/year (Fig. 1), by including China (66%), India (14%), Brazil (7%), Turkey (3%), Canada (3%) and North Korea (3%ee Table (1). Globally, most natural graphite is used in electrodes, refractories, lubricants, foundries, batteries, graphite shapes, recarburizing, steelmaking, and friction products such as brake linings (Fig. 2). Refractory and high-technology applications make graphite a critical material in industrialized countries. High-technology uses of graphite represent a portion of the market with fastest forecasted growth.

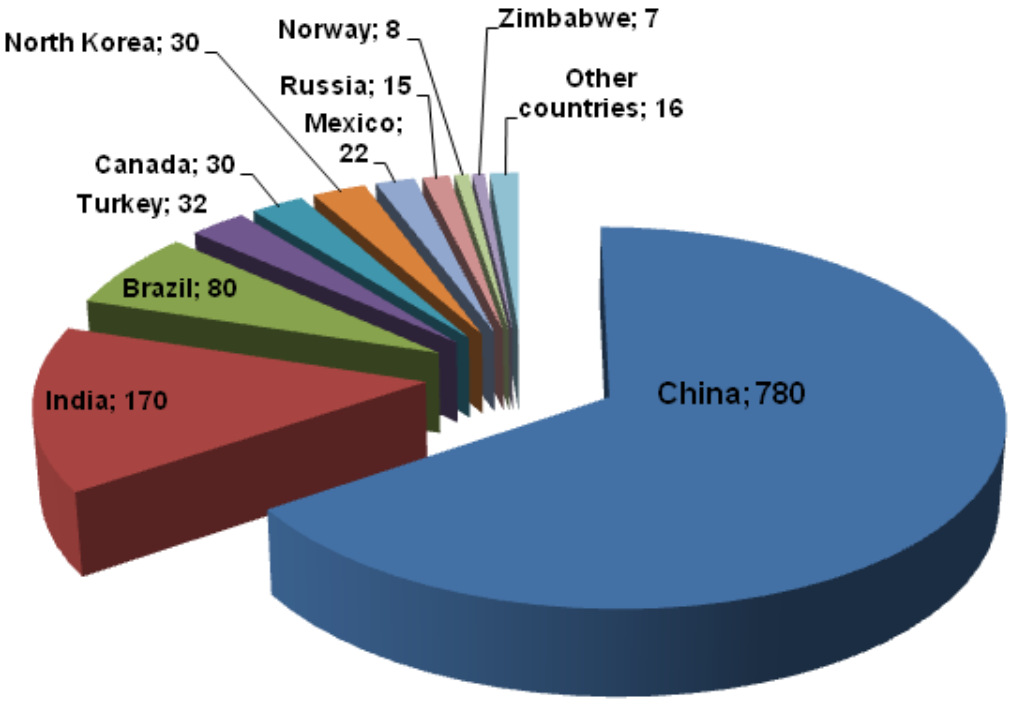

Figure 1. *Global graphite production, in thousands of tons, totaling 1.19 million tons, for 2015. Based on data from Statista (2015).*

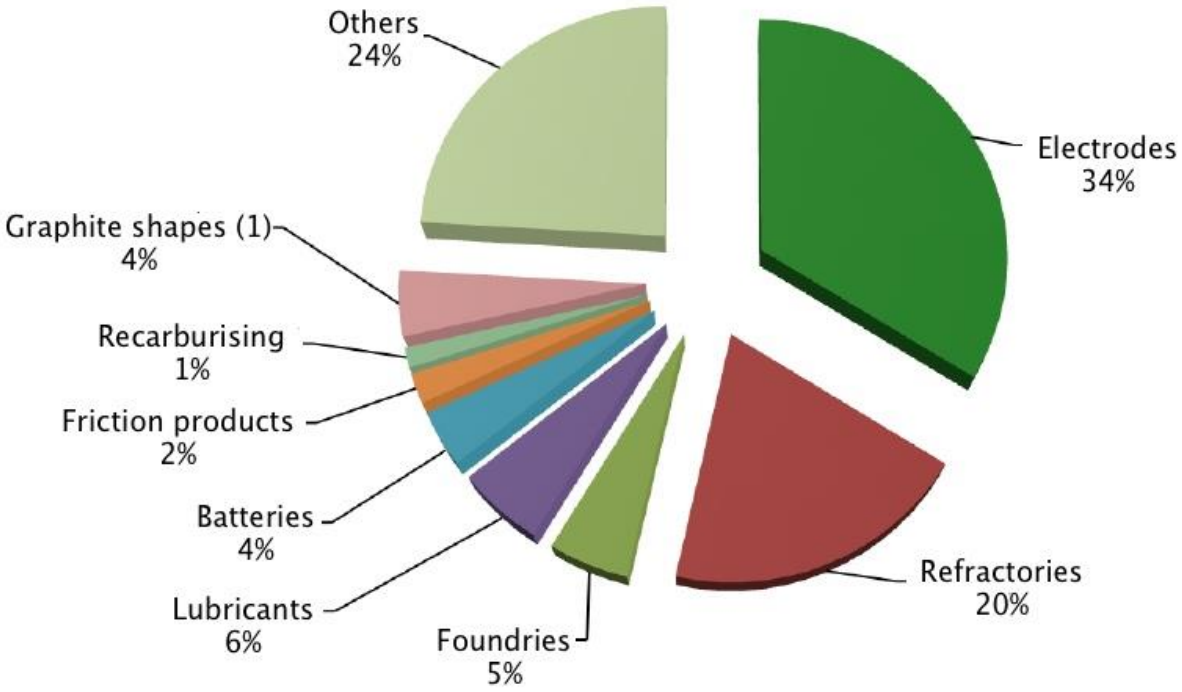

Figure 2. *Main uses of graphite for 2012, Based on Roskill Information Services | April (2013).*

Table 1. *Natural graphite production in 2015, Source: US geological Survey, 2016*

Country	Mine production 2015		Type of Graphite
	Ktons	Percentage	
China	780	66 %	Amorphous, Flake
India	170	14 %	Flake
Brazil	80	7 %	Flake
Turkey	32	3 %	Amorphous
Canada	30	3 %	Flake
North Korea	30	3 %	Amorphous, Flake
Mexico	22	2 %	Amorphous, Flake
Russia	15	1 %	Amorphous, Flake
Norway	8	1 %	Amorphous, Flake
Zimbabwe	7	1 %	Flake
Ukraine	5	0.4 %	Flake
Madagascar	5	0.4 %	Flake
Sri Lanka	4	0.3 %	Flake, Vein
Other countries	2	0.2 %	
World Total	1190		

1.2 Background, geological setting and purpose

Joutsijärvi study area is located in the eastern part of the Central Lapland Granitoid complex, about 25 km east from Kemijärvi. The Joutsijärvi area, strongly granitized schist belt, was earlier GTK's exploration target for base metals and gold (Pankka, 1999). Twenty two (22) shallow diamond drill holes (656 m totally) and six deep diamond drill holes (625m totally) were drilled in magnetic and electromagnetic anomalies caused by iron sulphides and flaky graphite. Flaky graphite was noted and beneficiation tests were made from selected samples. The preliminary tests showed that the quality of graphite is good. In this recent study drill cores were reviewed and more detailed mineralogical and chemical analyses on the flaky graphite schists.

The Joutsijärvi study area includes two targets: Kuusi in the north and Joutsi in the south magnetic anomaly belt including two KKJ- map sheets: 3632 and 3634. The graphite-sulphide-schist belong to the Vuolijärvi suite, consisting sericite quartzites, biotite gneisses and skarn rocks and is bounded in the northeast by the Central Lapland granitoid complex and in the southwest archean tonalite migmatites. Graphite-bearing schist consist mainly of biotite, quartz, graphite, plagioclase (albite) and pyrrhotite

Graphite-bearing schist is possible to recognize on the aerogeophysical maps (Figs 4, 5). Because they have higher electrical conductivity and magnetism than surrounding gneisses. The positive anomalies are caused by graphite and iron sulphides.

The aim of this study are (1) to determine the abundance of high-grade flaky graphite showing a well-ordered crystal lattice, thus suitable for industrial and technological use, (2) describe the geological setting and the petrography of the graphite ores from the selected drill core samples and (3) describe the results of recent beneficiation tests and mineral characterization geochemical results of the graphite ore.

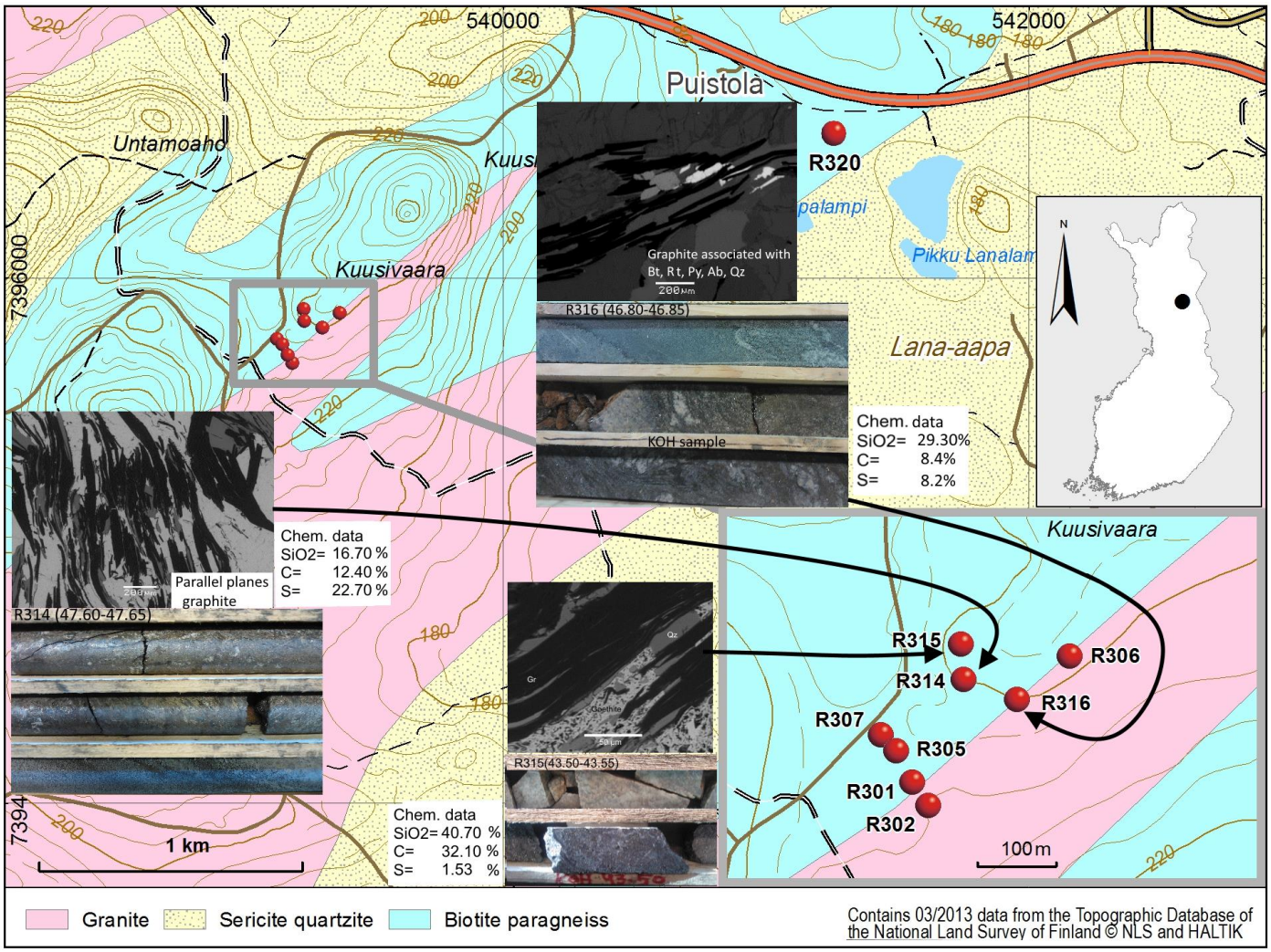

Figure 3. Figure 3. *Geological map showing the location of selected graphite-bearing drill core samples in Joutsijärvi area.*

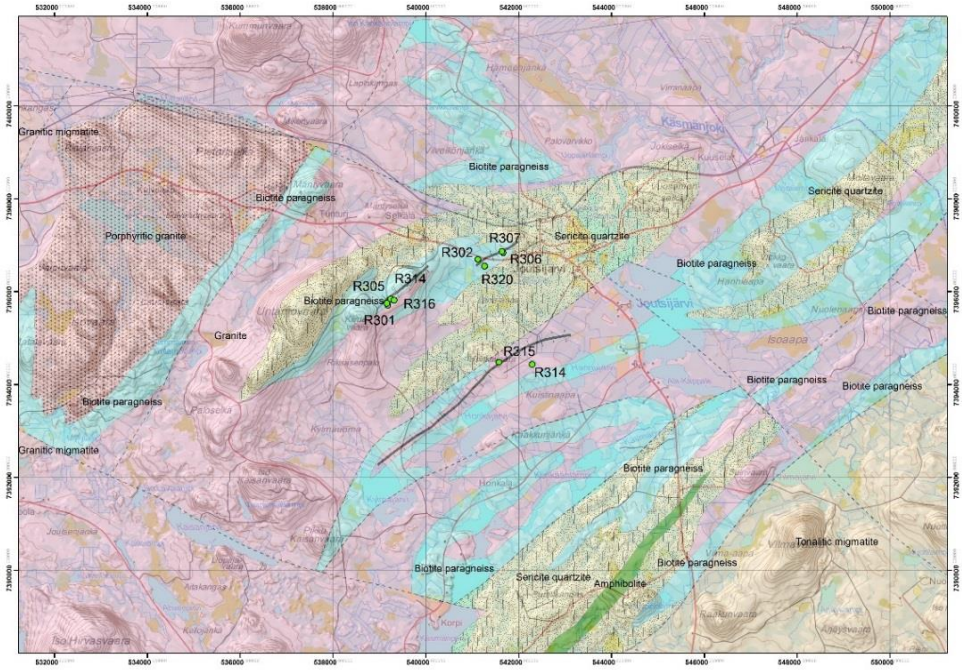

Figure 4. *Geological map of the area showing location of studied drill holes and selected graphite samples.*

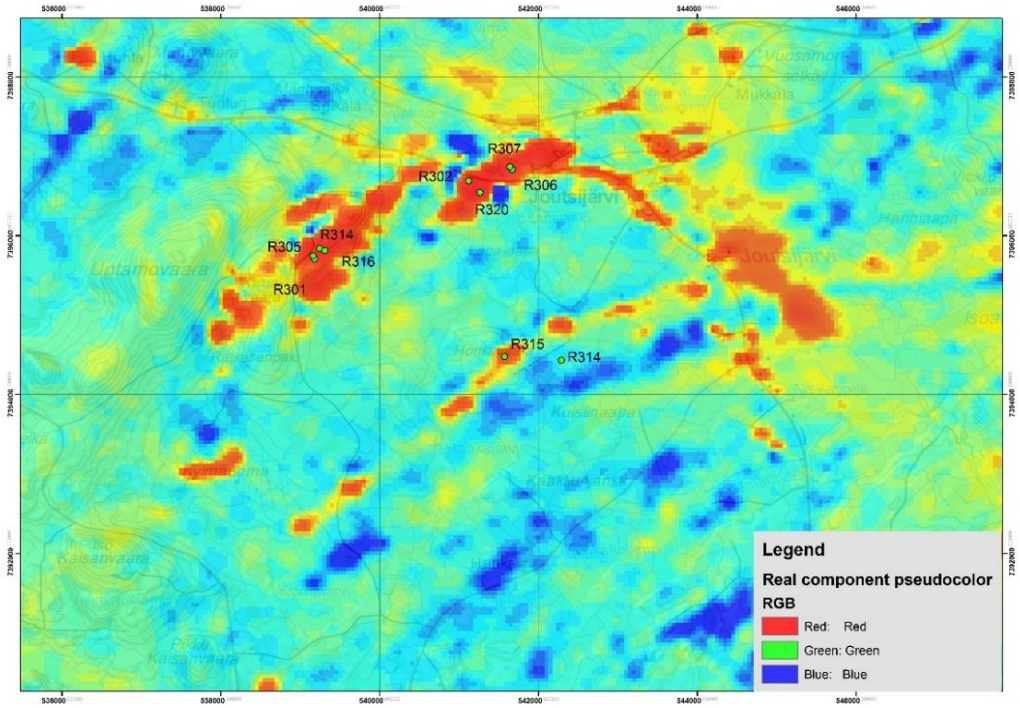

Figure 5. *Aeroelectromagnetic map of the Joutsijärvi area.*

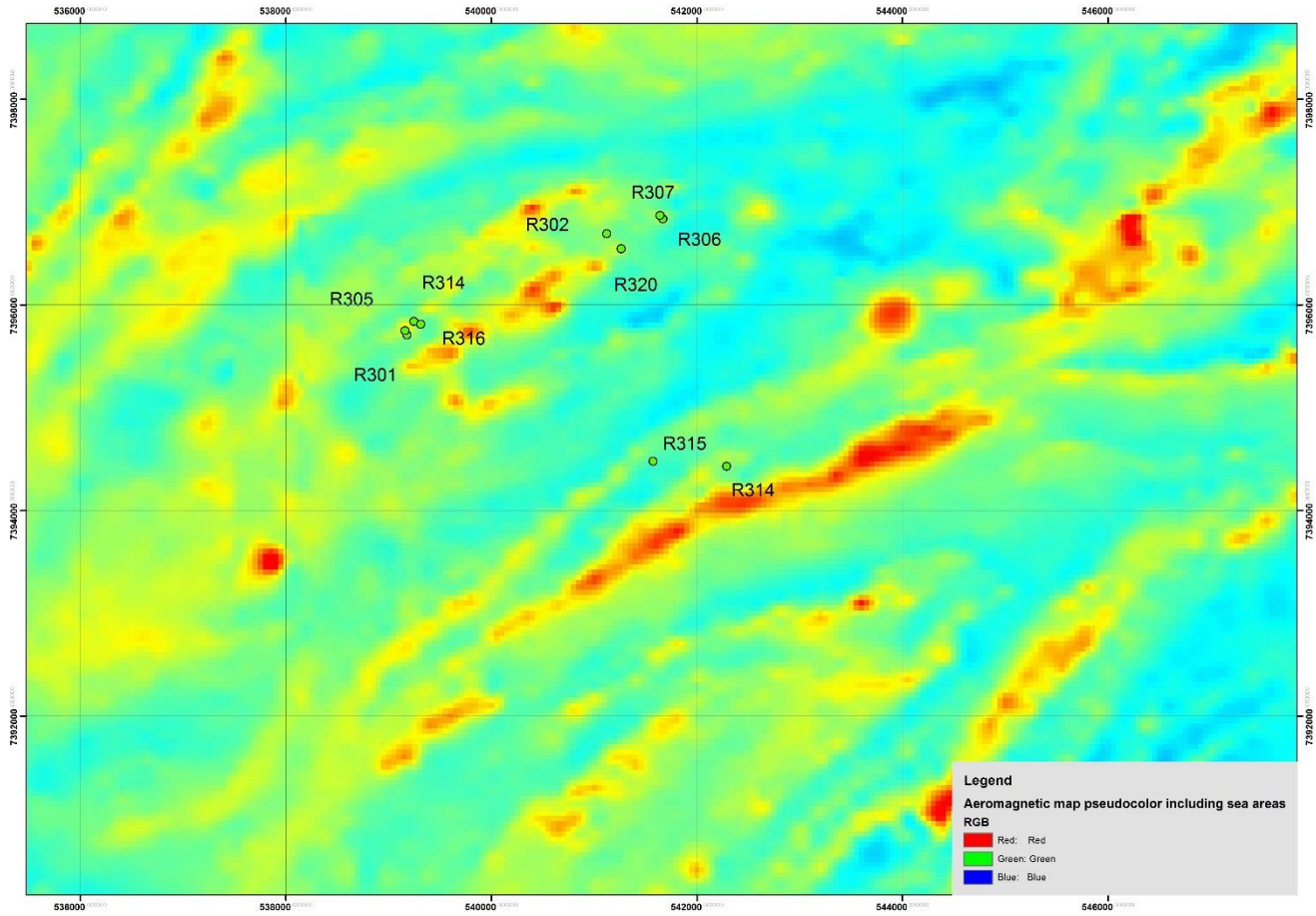

Figure 6. Aeromagnetic map of the Joutsijärvi area and the studied drill cores.

2 ANALYTICAL METHOD

Twenty three drill core samples were submitted to GTK Mineralogy Laboratory for polished thin section preparation and petrographic description. The samples for mineralogical studies were selected from eleven drill holes drilled from the Joutsijärvi area (KKJ map sheets 3632 and 3634).

The petrographic studies were carried out from the graphite rock samples to measure the microstructures, texture, and mineralogy and to some extent paragenesis of the graphite and associated minerals, by using ore microscope with reflected and transmitted light at different magnifications such as 2.5X, 5X, 10X and 20X objectives. About 20 sections were examined by using a Petrographic Microscope (LEICA DMLP) equipped with a digital camera (Leica).studied.

Scanning electron microscopy (SEM) in secondary electrons (SE) and back scattered electron (BSE) imaging modes was used to locate graphite at the surface of the thin section and to characterize the composition of the associated minerals by energy. These analyses were performed at the Mineral Processing Laboratory (GTK) - Espoo with a JEOL JSM 5900 LV field-emission SEM with a fully automated EDS and BSE detection system. Standard operating conditions for SEM imaging and EDS analysis were a 15 kV accelerating voltage potential and an electron beam current of 0.5 or 1 nA. Energy dispersive X-ray microanalysis on a SEM using the INCA x-sight EDS detector and INCA energy hardware to provide accurate determination of the composition of materials, which works for all types of studied samples and conditions.

X-ray powder diffraction data were collected for five selected samples using a Bruker D8 Discover A25 diffractometer with Cu-Ka radiation at Mineral Lab of GTK_Espoo. The operating conditions were, accelerating voltage 40 KV; current 40mA; scanning speed 0.2/sec; chart speed 60 mm/min and slit system having 0.5 mm width at the source side and 0.05 mm width at the detector side.

Whole-rock samples were analyzed by Labtium Analytical Laboratories (Kuopio), major and minor elements of drill core samples were determined by XRF (Method 175X) and determination of the rare earth elements and trace elements by ICP-MS (Method + 511P). Whole-rock samples were also analyzed for total sulfur and carbon by using high temperature (LECO) combustion technique with S/C analyzer (Labtium methods 810L and + 811L respectively). Loss-on-ignition (LOI), Labtium methodology (816L) procedure was used to run the LOI test in the studied samples.

3 PETROGRAPHIC ANALYSIS

Graphite generally occur in strongly foliated schist in which the foliation is defined by the parallel orientation of graphite flakes (Fig. 6). The foliation-laminae of the studied rocks consisting predominantly of biotite plus graphite lamellae alternate with quartz plus albite laminae. The studied schist rocks are marked by a rather consistent mineralogical composition marked by the abundance of biotite, quartz, albite and K-feldspar, associated with graphite, chlorite, pyrrhotite and pyrite. Few grains of rutile, zircon, ilmenite and monazite are present.

Biotite occurs in all studied samples; biotite is evenly distributed throughout specimens but occurs in different grain sizes. Most biotite forms tabular large subhedral grains, 500-2000 microns in size, and is always associated with graphite and sulfide grains. It is sometimes columnar and lathlike, commonly conspicuously restricted to the foliated parts of the rock (Fig. 7a, b). Representative chemical analyses of biotite by SEM with an average of SiO2 (42 wt %), Fe2O3 (8.5 K2O (8.9 wt %), Al2O3 (16.5 wt %), TiO2 (2.5 wt %) and F (1 wt %). Analyzed biotites are distinctive in their wide range in composition: Fe/(Fe+Mg) ranges from 0.024-0.47.
In the studied rocks, chlorite flakes, as a product of alteration of biotite, interleaved with, or completely replacing biotite flakes which are found in nearly most of the studied samples (Fig.7c, d). Based on SEM analysis, chlorite is closely related to composition of its host with some chemical changes: decrease in

SiO2, K2O and TiO2; increase in Al2O3 relative to biotite. Representative chemical analyses of chlorite by SEM with an average of SiO2 (51 wt %), Fe2O3 (9.5 wt %) K2O (1.2 wt %), Al2O3 (19.4 wt %), MgO (15 wt %) and H2O (>10%).

Quartz is frequently intergrown with albite. Quartz is usually anhedral and granular showing a recrystallized mosaic texture, while albite is subhedral and sometimes platy. Quartz and albite form distinct layers that alternate with biotite and chlorite (Fig. 7e, f). K-feldspar occurs sporadically as phenocryst (~300-700 µm) sub angular grains displaying typical Carlsbad twinning.

Pyrite and pyrrhotite are the dominant sulphides of the studied rocks. Within the rock groundmass they occur as coarse porphyroblasts, up to 900 µm grains or assemblages showing a preferred orientation parallel to foliation and schistosity of studied graphite mica schist rocks (Fig. 7g, h). The grain size of pyrite-pyrrhotite does not systematically change as a function of metamorphic grade. Both minerals also occur as joint fillings, subeuhedral pyrite is abundant and often associated with associated mainly with graphite and biotite (Fig. 7g, h). Pyrite and pyrrhotite are seen in close contact with each other. Chemical analyses of both pyrite and pyrrhotite by SEM analyses indicated little variation of Fe and S content in each case. Fe composition varies from 31.4 to 42.7 wt% and S varies from 48.2 to 62.1 wt% in pyrite, while in pyrrhotite Fe content between 56.3 to 58.7 wt% and S content between 38.4-39.7 wt percent. Pyrrhotite grains appear with a lighter color than pyrite on the BSE image due to its higher atomic density, with iron content higher and sulphur content lower than for pyrite. Little chemical variation or departure from pyrite and pyrrhotite ratios change during metamorphism as prograde heating results in sulphur release from pyrite to form pyrrhotite and as retrograde cooling permits re-growth of pyrite as the pyrrhotite releases sulphur (McClay and Ellis, 1983). Pyrite also forms mosaic textures with 120 ~ triple junctions between large pyrite porphyroblasts show the growth of irregular pyritic mass in the later deformation. Pyrrhotite in pyritic ores has often been attributed to the breakdown of pyrite during metamorphism. It is now clear that pyrrhotite can be primary and that the presence of pyrrhotite with the pyrite provides a buffer that constrains sulphur activity during metamorphism (Tiwary and Cook, 1998).

Rutiles occur as polycrystalline aggregates, which are characterized by a fine-grained intergrowth of rutile and zircon (Fig 8a). The rutile grains can show euhedral to subhedral forms, associated with monazite with grain sizes from 50 µm up to 100 µm (Fig 8b), also rutile forms mainly single crystals in the matrix but also occurs as inclusion in other minerals such as biotite and quartz and ilmenite (Fig. c, d). Ilmenite occurs as subhedral to euhedral lath-like or prismatic crystals up to several microns long (>100 µm) and mostly associated with biotite and quartz (Fig 8c, d).

SEM results indicate that monazite is the principal REE-bearing minerals in the studied samples. Monazite appears as isolated minute crystals with a diameter 50—200 µm (Fig. 9). Multigrain analyses show that the monazite- (Ce) is rich in LREE as Ce (~33%), La (~18%), Nd (~9.0%), CaO (1.5%), P2O5 (31.5%), Th (~5%) and F (<1%).

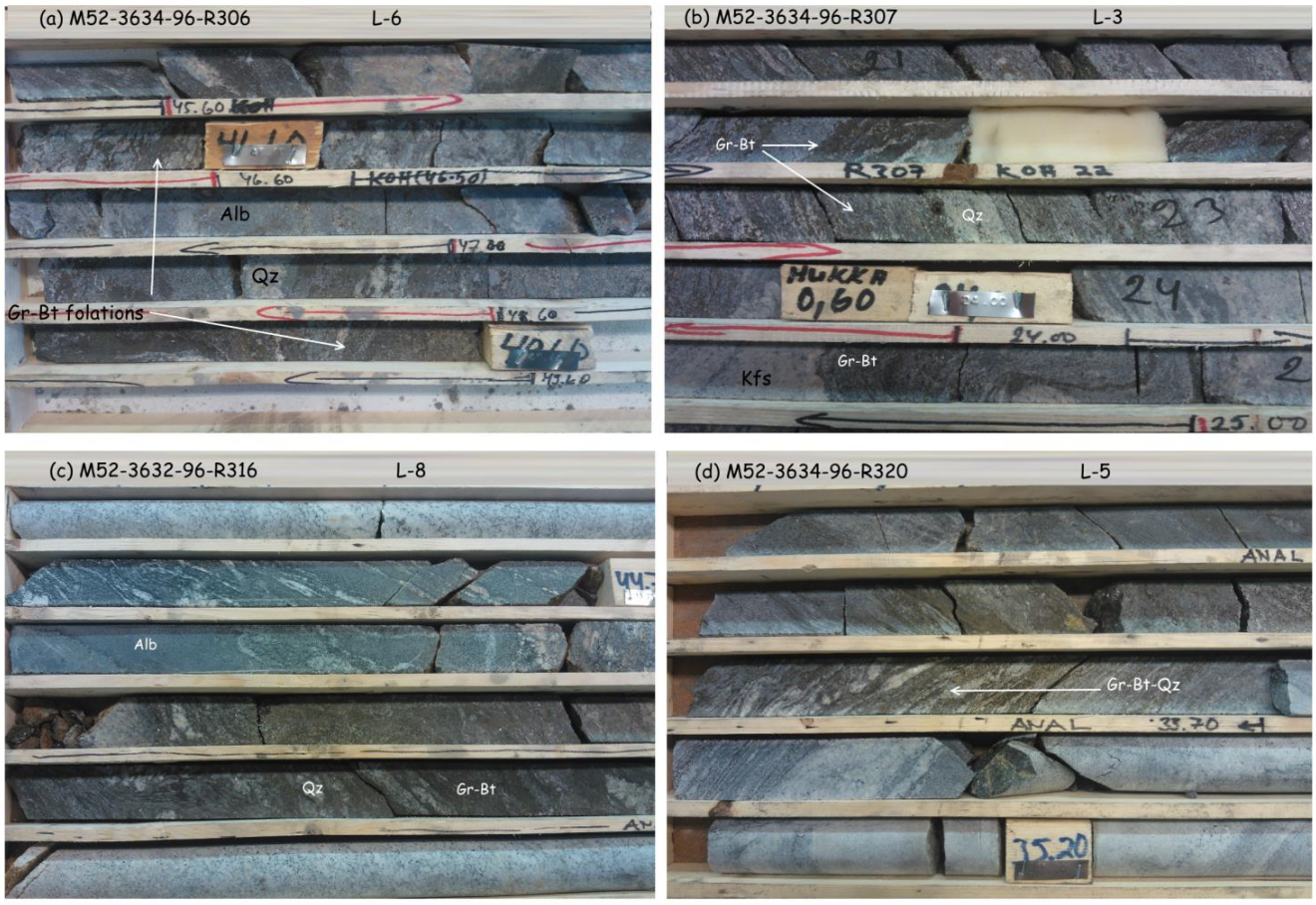

Figure 7. *Drill core photographs of biotite schist and alternating rocks, (a, b) Typical appearance with well-developed bedding parallel foliation of graphite (Gr) and biotite (Bt). Microscope studies reveal that quartz (Qz), K-feldspar (Kfs) and albite (Alb) (light colored laminae) alternated with biotite and graphite to define the lamination. (c, d) Graphite schist alternated with granitic gneiss rocks to show that foliation is generally parallel to original bedding and lineation is generally parallel to major fold axes.*

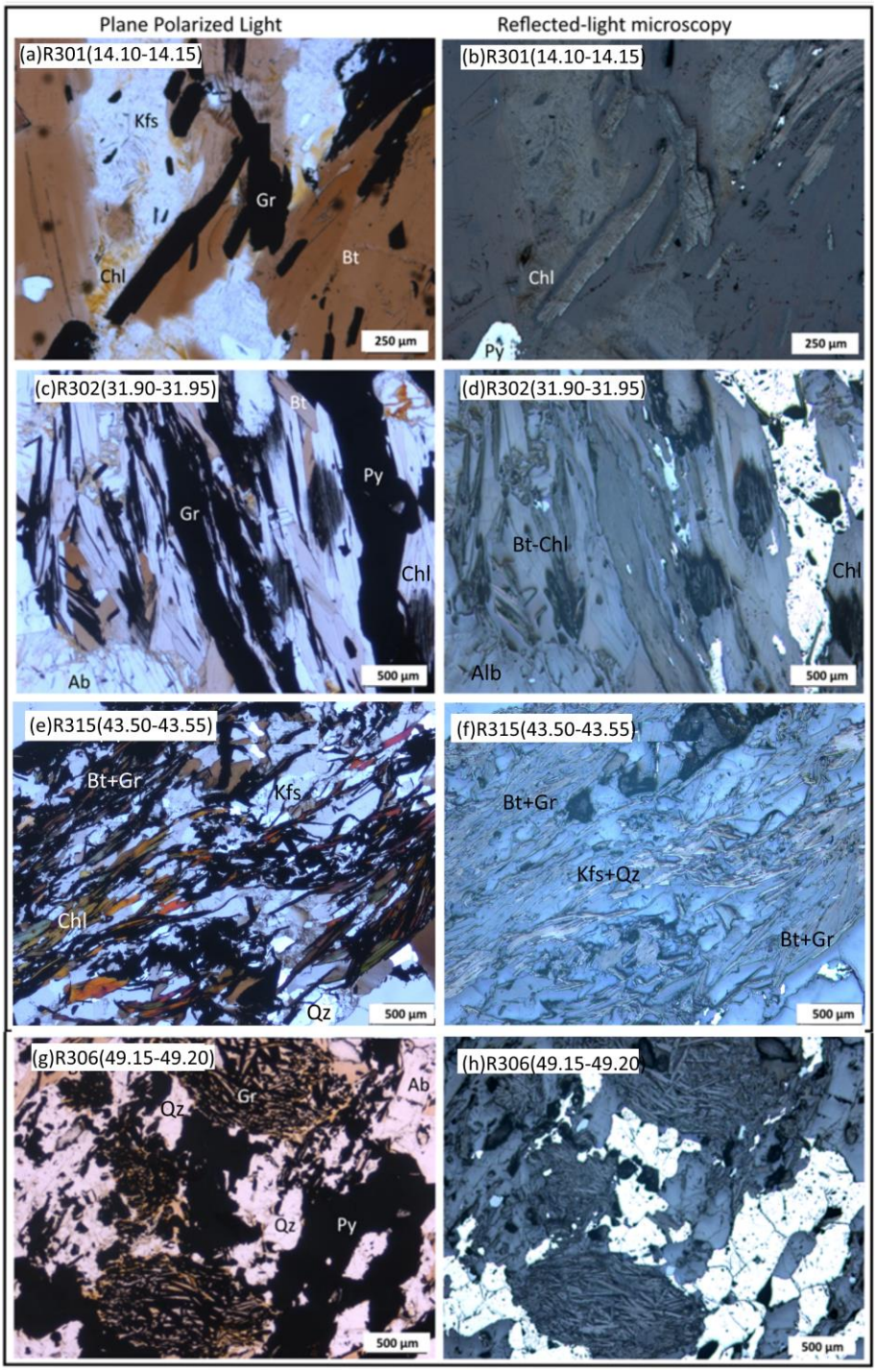

Figure 8. *Photomicrographs illustrating different petrographic features of graphite-bearing schist, (a, b) Graphite (Gr) flakes with biotite laths, often restricted to the well floated parts of the rock, (c, d) Schistosity exhibited by parallel arrangement of graphite flakes interbanded with biotite (Bt) and chlorite (Chl), (e, f) Schistosity of quartz (Qz) and K-feldspar (Kfs) within graphite schist (g, h) Graphite (Gr) flakes and biotite (Bt) occur as randomly oriented lathes within quartz (Qz) and pyrite (Py) groundmass.*

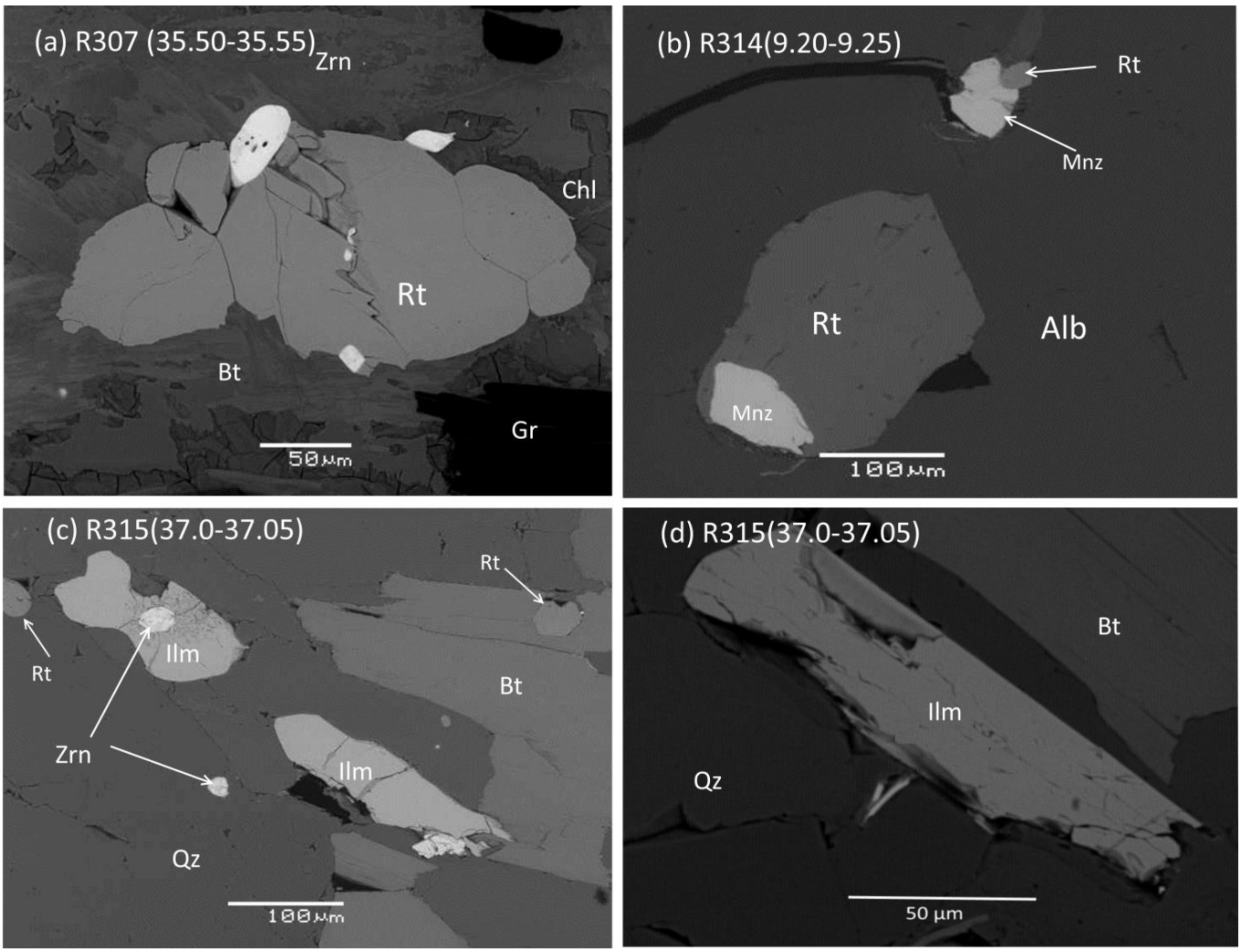

Figure 9. *Backscattered electron (BSE) images of some accessory minerals (a) Multiple equant rutile (Rt) crystals (light gray) associated with zircon (Zrn), (b) Subhedral rutile grain and monazite within albite(Alb), (c) Lathlike grains of ilmenite(Ilm) associated with biotite zircon and rutile, (d) Bladed ilmenite(Ilm) within quartz.*

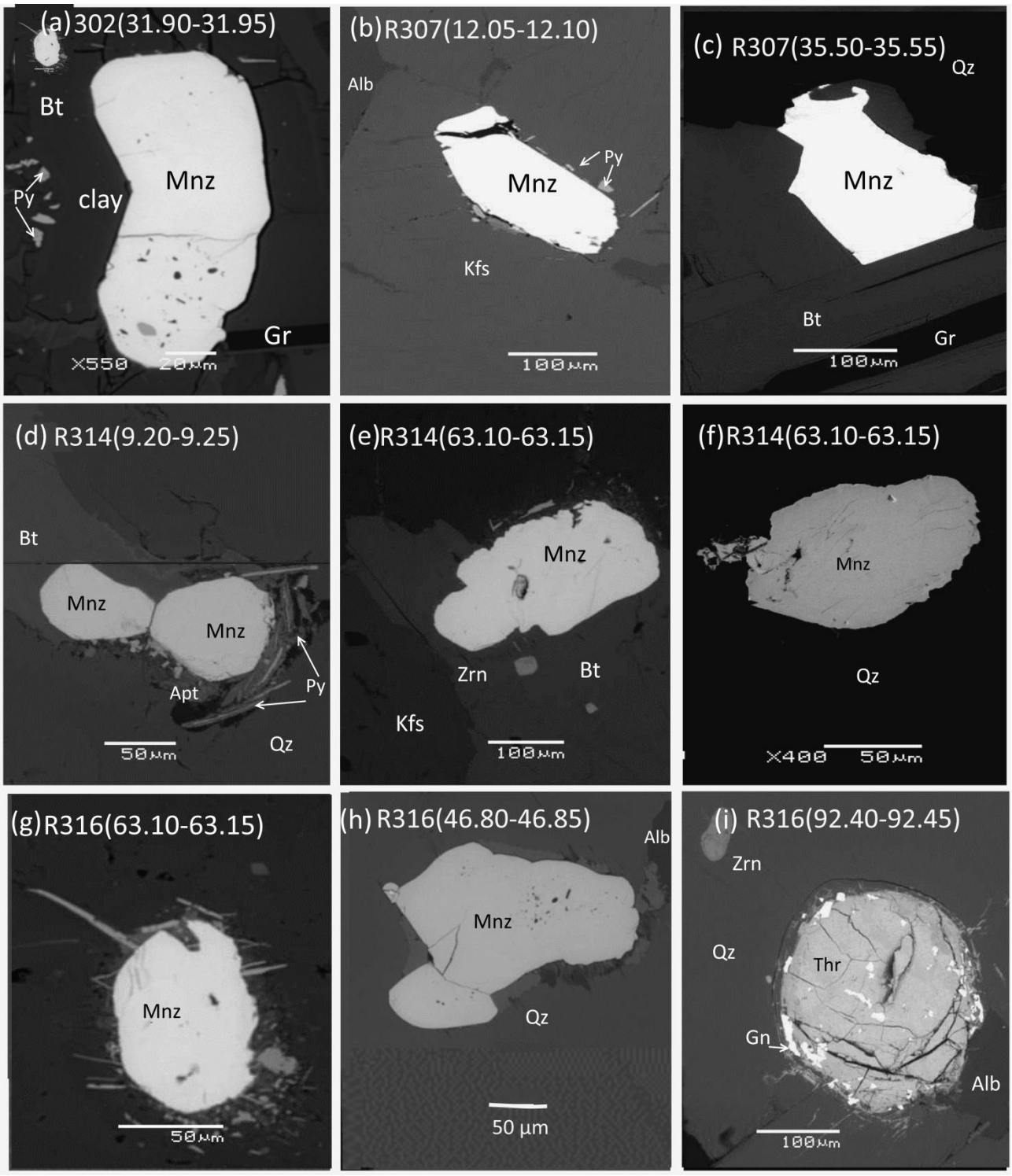

Figure 10. *Backscattered electron (BSE) images of multiple monazite (Mnz) grains with different form and size.*

4 GRAPHITE MINERALOGY

4.1 Graphite morphology

Petrographic examination of polished thin sections (Figure 7) using an optical microscope is a relatively affordable and quick way of estimating the in situ graphite flake size distribution and likely liberation characteristics. A representative selection of thin-sections was complemented by methods such as quantitative evaluation of minerals by scanning electron microscopy (SEM) and mineral liberation analyzer and X-ray diffraction (XRD).

In graphite gneiss and graphite-mica schist the foliation is defined by the parallel orientation of graphite flakes. The gangue minerals are biotite, quartz, albite, K-feldspar pyrite and pyrrhotite with subordinate chlorite and clay (Fig, 10). The graphite flakes are situated interstitially between grain boundaries of gangue silicates, and more rarely as inclusions in the silicate minerals. Graphite flakes have no inclusions

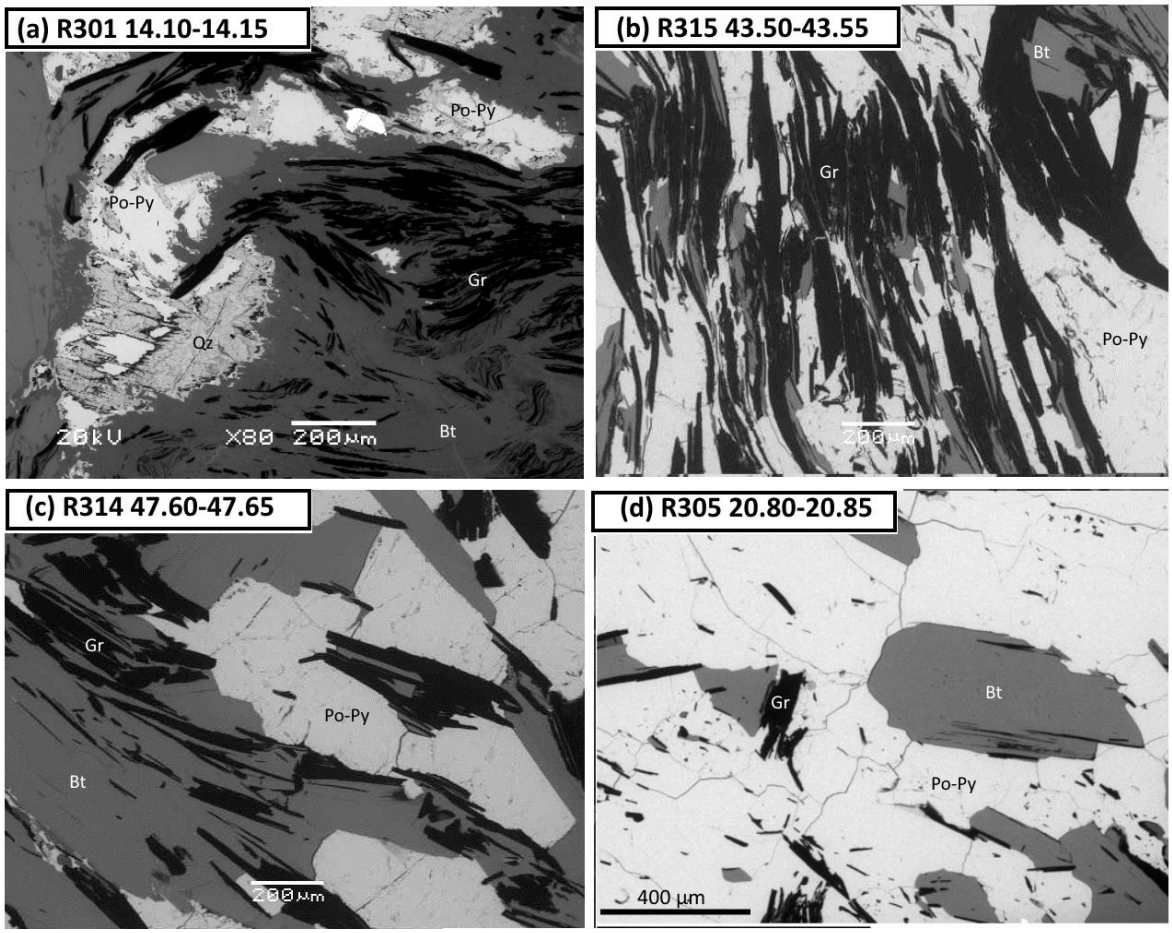

Figure 11. *Backscattered electron (BSE) images show graphite flakes, (a, b) the graphite(Gr) flakes oriented parallel to foliation, (c, d) the images show the foliation and distribution of sulfide and other minerals identified pyrite (Py), pyrrhotite(Po) and biotite(Bt)*

Characterization of size and morphology of the graphite flakes is therefore important in ore evaluation (Fig. 11). Due to dominating of graphite flakes in most of studied rocks, the graphite flakes were aligned at high-grade regional or contact metamorphism. Later deformation conditions graphite-bearing schist demonstrated by strong wavy parallel planes of graphite and sub-basal deformation lamellae of biotite as well as by fine grain boundary suturing and beginning recrystallization of quartz (Fig. 11c, d).

This involves the acquisition of digital images of the thin sections and, morphological parameters such as area, perimeter, longest and shortest axes, etc., of mineral grains are recorded. The dominating size of the graphite flakes is 100 µm 2000 µm and graphite shows good orientation with flakes frequently in mean length of 500 µm. Most graphite flakes are oblong shaped, but not particularly fibrous, and the ratios between their long and short axes are in the range of 2 to 4 for the majority of the flakes. These results are typical for Kuusivaara graphite and are also characteristic of a coarse, high-quality, flake graphite ore. Aggregate measurements from several thin-sections are usually necessary to give a statistically significant description of the ore. An example of the results of such measurements is shown in (Fig. 12a, b) which shows aggregate grain morphological measurements of the graphite ore.

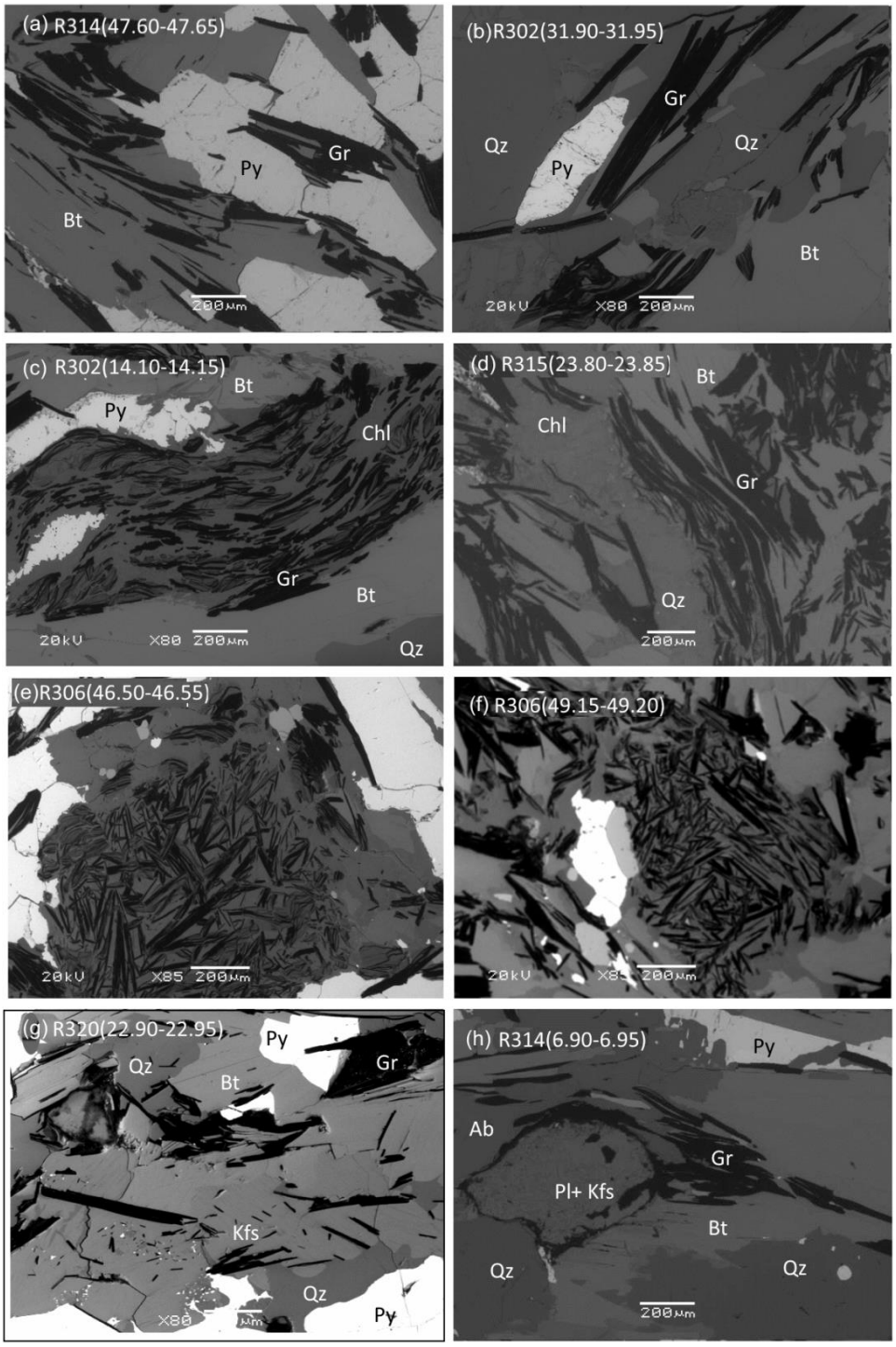

Figure 12. *Backscattered electron (BSE) images show the foliation and distribution of sulfide and other main minerals, (a, b) the graphite distribution with sulfide and other minerals identified pyrite (Py), pyrrhotite (Po) and biotite (Bt), (c, d) wavy parallel planes of graphite (Gr) flakes within the biotite schist rock, (e, f) aggregates of graphite (Gr) flakes parallel and perpendicular to foliation*

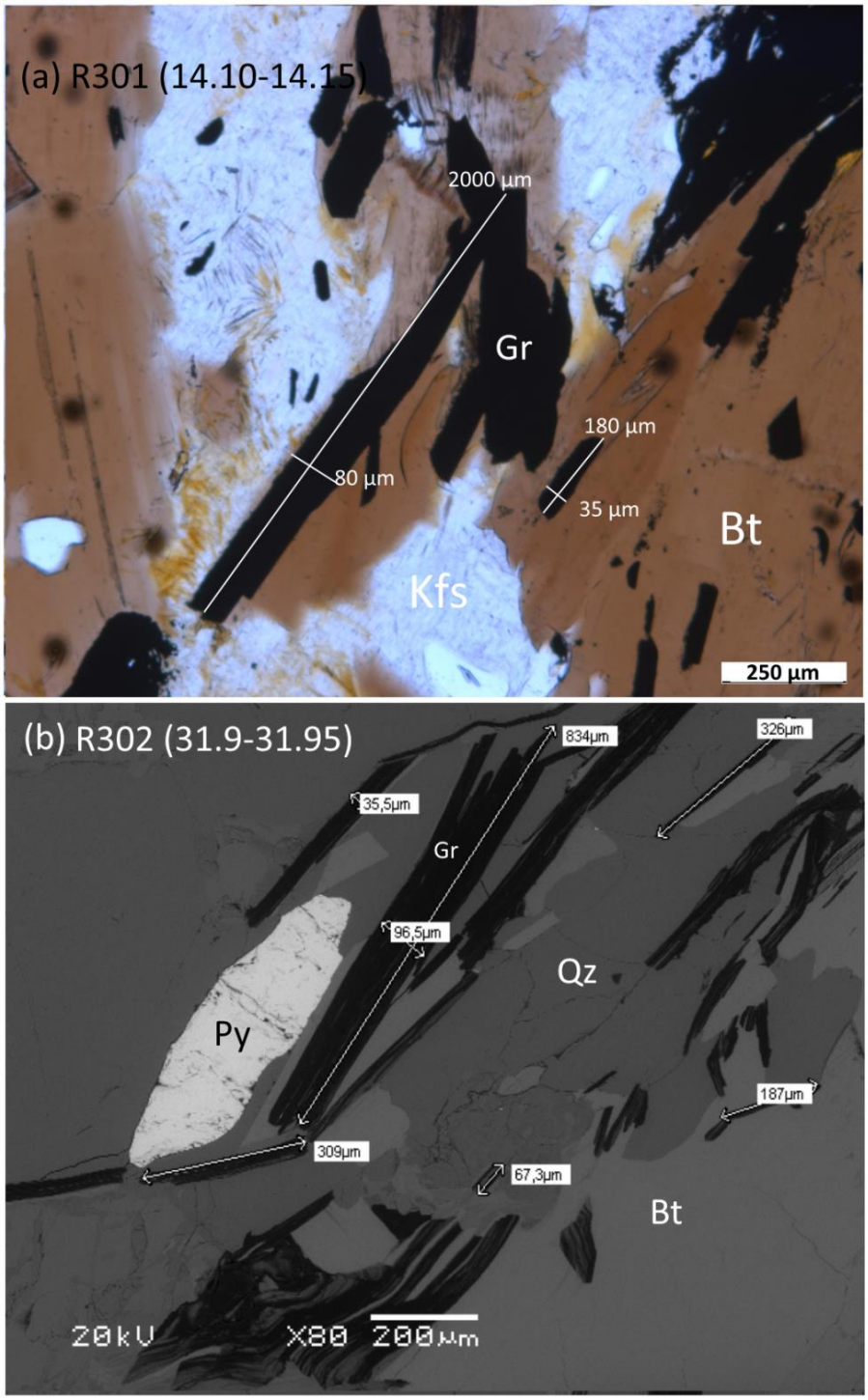

Figure 13. *Determining the size and shape of the graphite flakes, (a) Photomicrograph under cross polarized light and (b) BSI microphotographs illustrating graphite textures, the graphite shows good orientation with flakes frequently in excess of 1000 micron in length and with widths typically up to 30 micron or more, with a population of pyrite (Py), biotite (Bt), K-feldspar (Kfs) and quartz (Qz) minerals within the graphite schist.*

Thin section examination highlighted that there were two graphite populations, with the majority as coarse flakes but with a second population graphite of very small graphite flakes occurring as fracture, cavity fillings or as fissure fillings in veins. These veins with diameters of few microns and length can be from 2mm to 10 mm (Fig. 13).

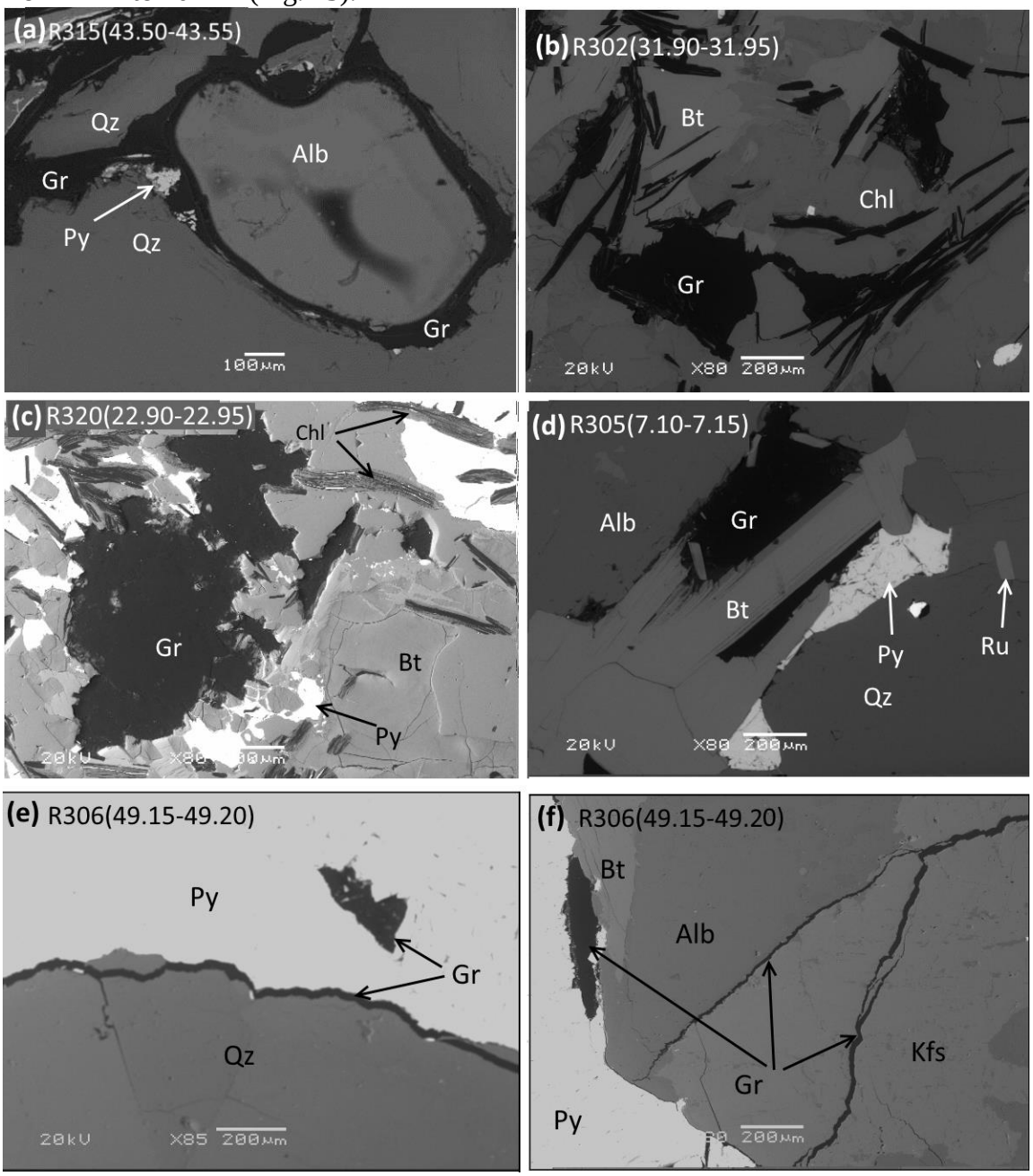

Figure 14. *Graphite* filling *cavities* or fissures *(a) graphite surrounded the albite grain (b, c, d) graphite filled a vug within biotite fracture around (e) graphite filled a fracture across the pyrite and quartz, (f) graphite filled a fracture within feldspar.*

The graphite grains are situated interstitially between grain boundaries of gangue silicates, and more rarely as inclusions in the silicate minerals. XRD analysis of graphite flakes shows that the d002 inter-layer spacing is 3.40 Å which is characteristic of fully ordered (crystalline) graphite, with a temperature of formation of above 700° C (Landis 1971, Katz 1987). Accessory minerals include rutile, ilmenite, monazite and zircon. Titanium is mainly present as rutile, mostly as grains occupying the matrix

4.2 Graphite crystallinity

X-ray diffractometry (XRD) was used to determine the crystallinity of the flake graphite and to check for potential impurities. The XRD data collection was performed by a Bruker D8 Discover A25 diffractometer. Powdered samples were scanned from 2-70 in 2θ range with 0.02° step interval and 2s/step counter time. Phases were identified with Bruker's EVA (4.0) software using ICDD (International Centre for Diffraction Data) database PDF-4 Minerals 2014 in GTK_Lab of mineralogy by Mia Tiljander.

High quality data on graphite using X-ray powder diffraction is difficult to obtain since carbon has a very low mass absorption coefficient for X-rays, which contribute to errors associated with displacement and peak broadening. Also, it is difficult to prepare a graphite samples, having a strong preferred orientation and less textured (Howe et al., 2003). To obtain better results, this survey focused on the analysis of the 002 peak that shows the greatest intensity in well-ordered graphite (Baiju et al. 2005).

The X-ray diffraction patterns of graphite samples are shown in figure (14), and the calculated structural data are presented in table (2). The 2θ, d values and full width of the peak at half-maximum are estimated from the diffractogram (Fig. 15). The crystallite size (Lc) along stacking direction is then calculated from Scherer's equation:

$$\mathbf{LC\ (_{002})\ =\ K\ \lambda /\ \beta\ (_{002})\ \cos\ \theta}$$

where K is the shape constant, assumed to be 0.9 (Griffin, 1967; Tagiri and Tsuboi, 1979) and β ($_{002}$) is the full width of the peak at half-maximum in radian and λ is the X-ray wave length in angstroms and 8 is the angle of diffraction in radian. Further the graphitization degree (DG) has been calculated from the equation (Tagiri, 1981):

$$\mathbf{DG\ =\ \{[d\ (_{002})\ -3.71]\ /\ [\log\ LC\ (_{002})\ /1000]\}\ x\ 100}$$

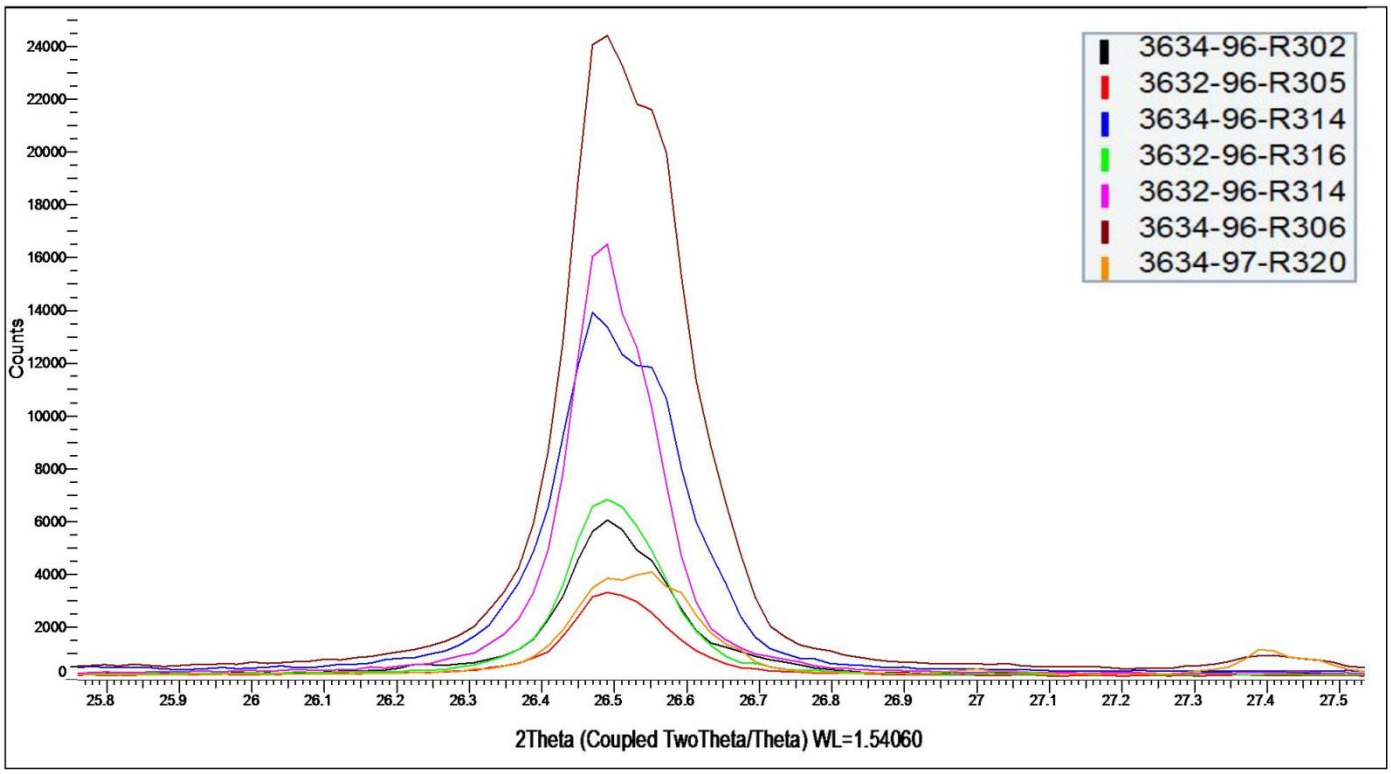

Figure 15. *Selected typical X-ray diffraction patterns of studied graphite samples.*

A binary plot of **LC (002)** vs. **d (002)** (after Tagiri and Oba, 1986) shows that the studied graphite samples belong to the well crystallized graphite phase (Fig. 16). On the plot showing the linear relationship between the metamorphic temperature and calculation DG values (Wada et al., 1994), the selected graphite samples of Kuusivaara-Joutsijärvi samples cluster around 520°C and 830°C (Fig 17). The metamorphic temperature of graphite crystallization for the present samples is particularly variable between (520-830°C), and may be an unreliable estimate of temperature due to excessive equilibration. When the stable isotope data are available, analysis of graphite thermometry will be useful in narrowing the peak temperature margins shown.

Table 2 Structural parameters extracted from the curve fitting of XRD of studied graphite samples

Sample	2θ°	d(002)Å	β(002) Å	Lc(002) Å	GD Å
3634-96-R302 31.90	26.50	3.361	0.154	589	147.30
3632-96-R305 20.80	26.50	3.360	0.146	621	164.55
3634-96-R306 49.15	26.51	3.359	0.176	514	118.02
3634-96-R314 24.00	26.50	3.361	0.187	485	108.14
3632-96-R316 46.80	26.50	3.360	0.145	627	167.77
3632-96-R314 47.60	26.49	3.362	0.133	684	205.04
3634-97-R320 22.90	26.53	3.357	0.185	490	110.57

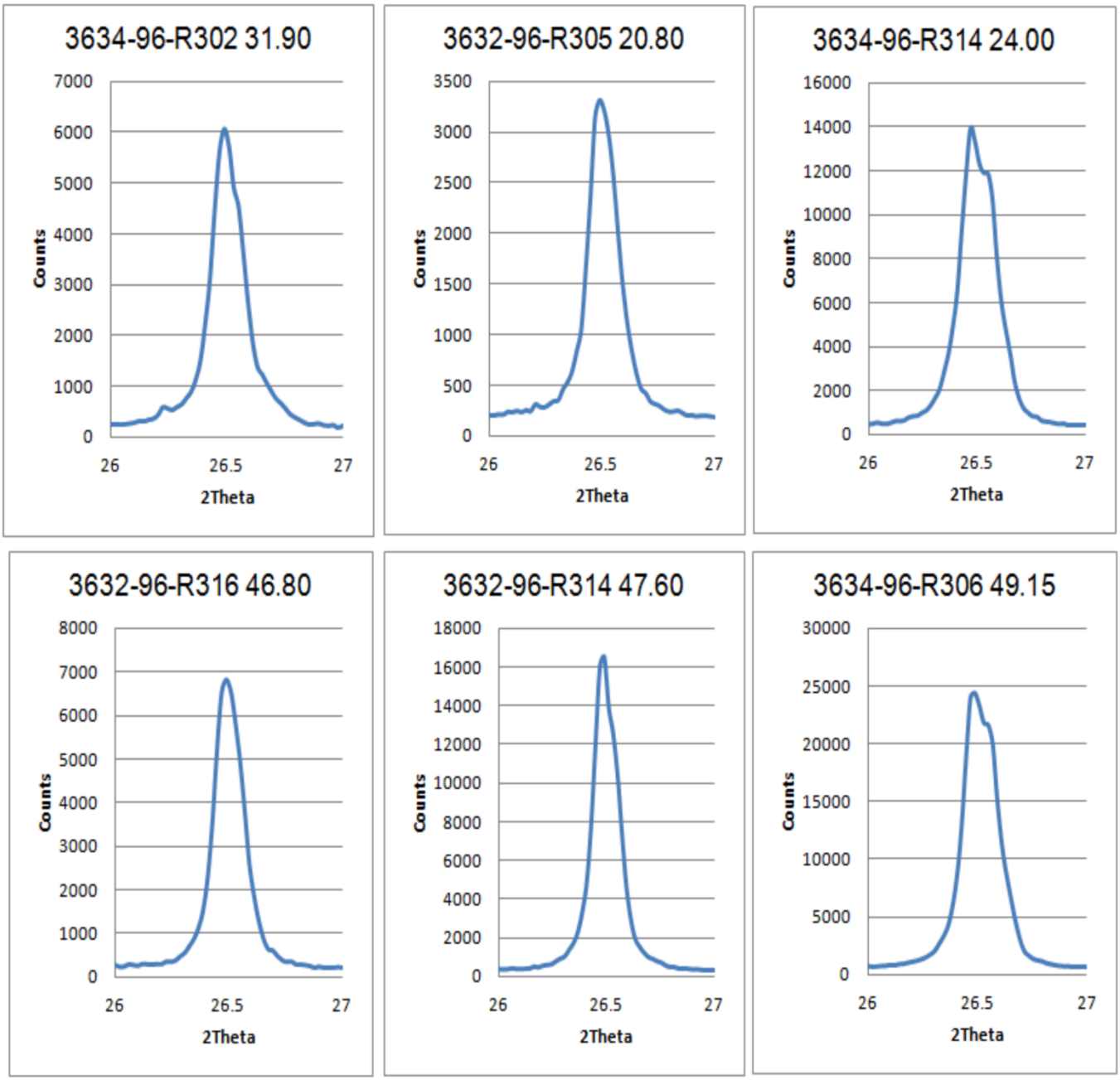

Figure 16. *X-ray powder diffraction (002) peaks of the selected graphite samples from the studied area.*

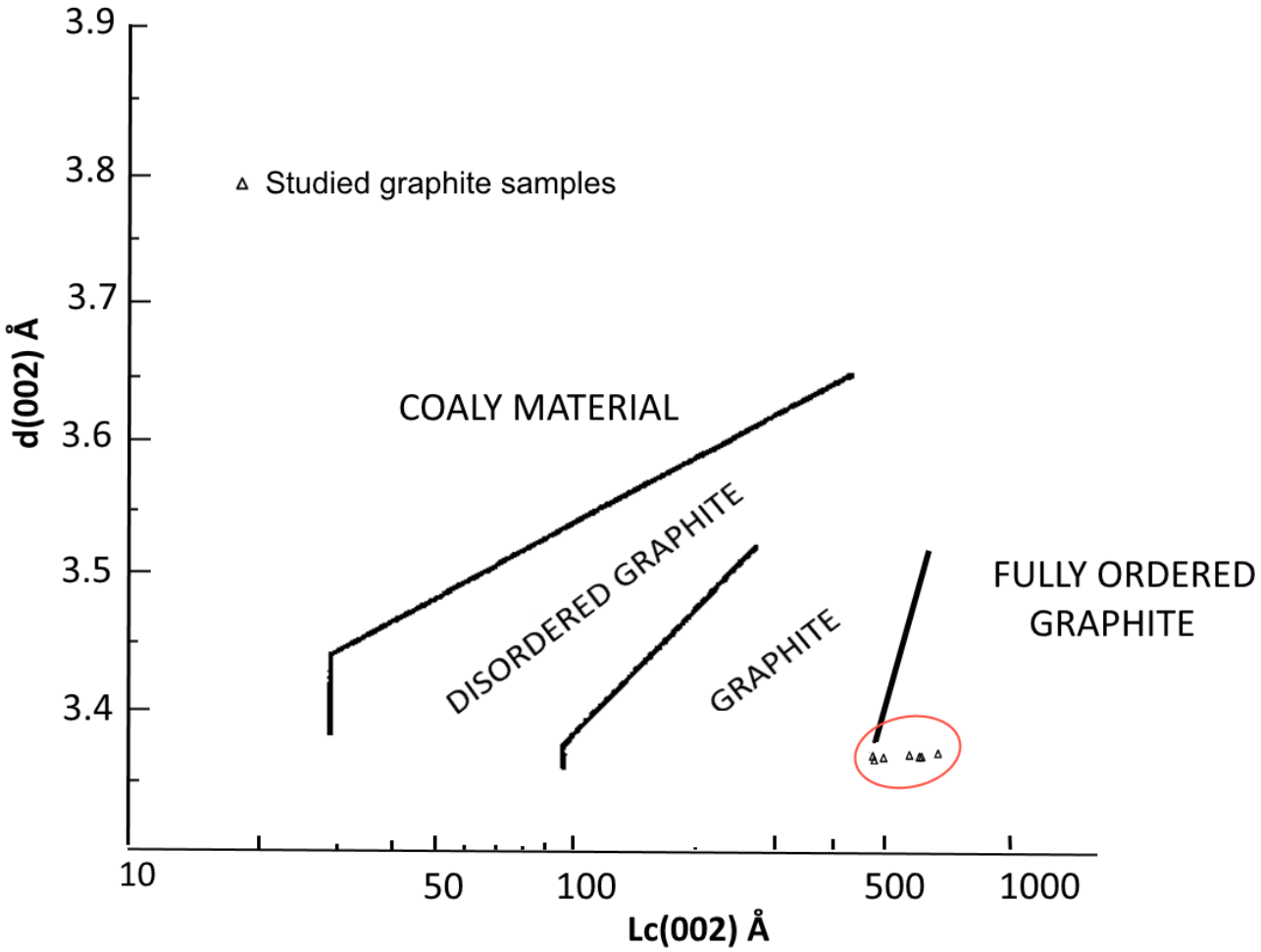

Figure 17. *Interplanar spacing d (002) vs crystallite size, Lc (002), for the some studied graphite samples (After Tagiri and Oba, 1986).*

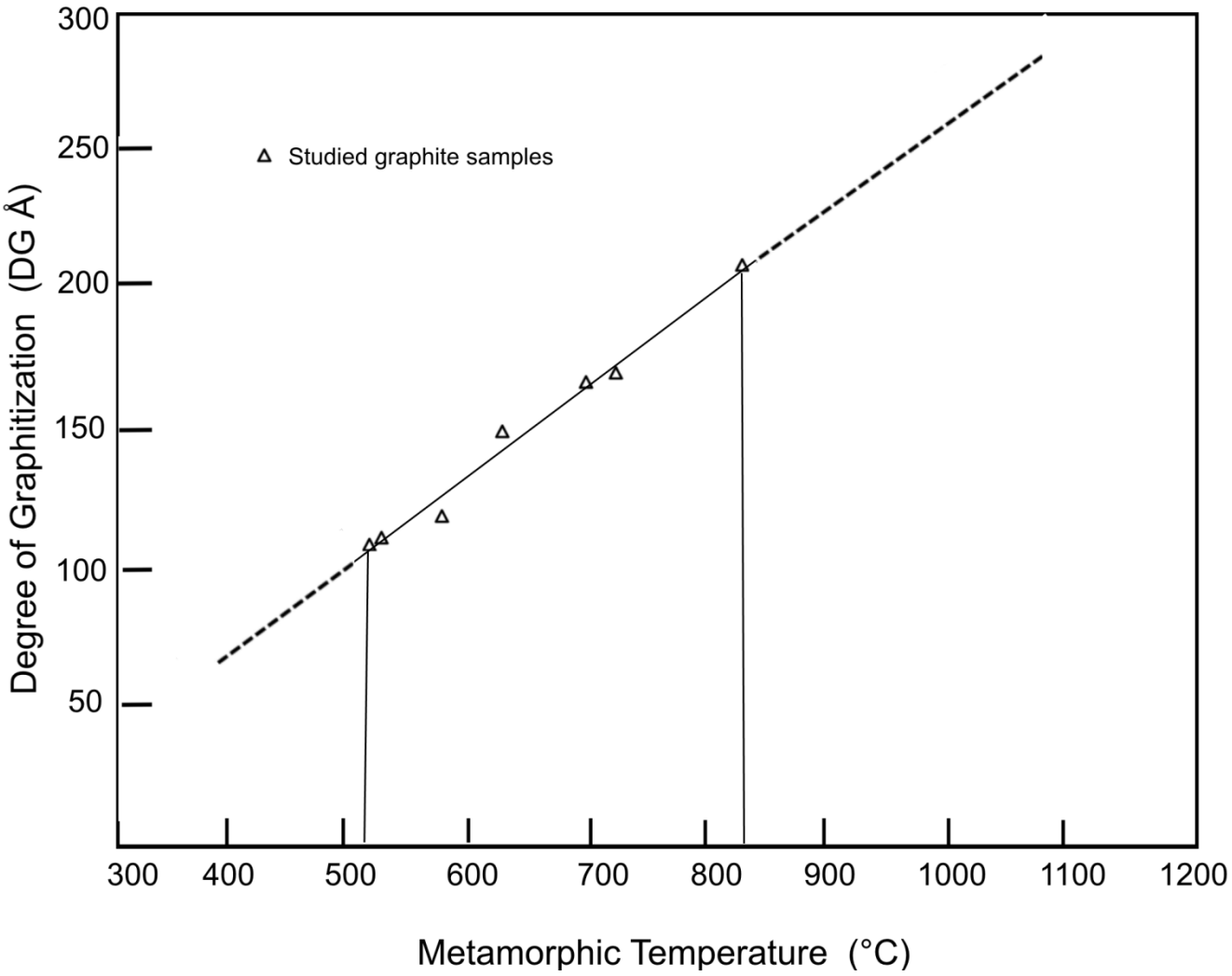

Figure 18. *Degree of graphitization of the selected graphite samples compared with the linear relationship for Wada et al. (1994). The derived temperatures for the studied graphite fall between 520°C and 830°C.*

5 GEOCHEMISTRY

Chemical analyses of the 10 graphitic sulfide-rich schists are listed in Table 3. The sum of metal oxide, sulphur, and carbon weight percent is greater than 100. Sums greater than 100 are an artefact of representing total iron as an iron oxide rather than as a combination of iron oxide and iron sulphide (Ferry, 1981). Loss-on-ignition is a common method to estimate carbon and carbonate contents in studied samples.
Table3. Whole-rock chemical data for selected graphite-rich schist samples.

Sample	R301 14.1–14.15)	R302) (31.90–31.95)	R305 (20.80–20.85)	R306 (49.15–49.20)	R307 (22.0–22.05)	R314 (24.00–24.05)	R314 (47.6–47.65)	R315 (43.50–43.55)	R316 46.80–46.85)	R320 (22.90–22.95)
Na2O	0.18	0.34	0.28	1.44	0.69	4.64	0.19	1.57	1.25	0.79
MgO	3.00	4.62	2.15	2.18	3.79	1.97	2.86	1.77	4.77	2.18
Al2O3	19.80	10.30	5.36	12.70	11.50	15.40	5.17	7.12	13.20	9.95
SiO2	34.90	26.20	11.50	32.10	32.00	51.20	16.70	40.70	29.30	35.80
P2O5	0.01	0.01	0.01	0.04	0.12	0.56	0.01	0.03	0.02	0.05
K2O	3.59	2.65	1.85	2.10	2.08	1.40	2.12	1.35	4.85	2.75
CaO	0.11	0.15	0.03	0.67	0.36	3.48	0.05	0.95	0.62	0.14
TiO2	0.91	1.10	0.51	1.20	0.55	0.64	0.69	0.53	1.44	0.46
MnO	0.02	0.03	0.02	0.01	0.01	0.02	0.02	0.01	0.07	0.01
Fe2O3	22	40	60	30	36	4.6	50	4.6	28	32
LOI	9.32	5.90	5.70	11.60	5.00	12.20	12.50	32.40	8.43	8.72
Total	93.84	91.30	87.42	94.04	92.10	96.11	90.31	91.03	91.94	92.85
S	8.73	7.52	27.80	14.10	16.60	1.69	22.70	1.53	8.28	14.50
C	9.15	5.88	5.61	11.50	4.95	12.50	12.40	32.10	8.41	8.69
Trace elements (ppm)										
V	579	736	582	520	649	134	753	149	696	471
Cr	194	164	90	110	198	129	143	96	232	92
Ni	177	328	422	285	343	122	433	126	155	279
Cu	431	637	827	349	677	295	831	203	499	1290
Zn	38	53	42	25	37	32	49	24	104	29
Rb	243	173	146	122	166	123	152	129	332	99
Sr	10	26	10	19	22	107	10	39	65	11
Y	21	10	10	13	75	28	10	10	21	32
Zr	154	142	82	131	55	119	119	41	178	76
Nb	20	20	20	20	20	20	20	20	20	20
Mo	44	27	50	24	10	10	46	10	22	21
Sn	30	38	37	30	30	30	37	30	30	30
Sb	50	50	50	50	50	50	50	50	50	50
Ba	343	185	279	135	126	93	157	83	521	230
La	30	30	30	30	30	30	30	30	30	30
Ce	55	80	33	42	64	57	71	30	36	30
Pb	30	30	30	30	30	30	30	30	30	30
Bi	30	30	30	30	30	30	34	30	30	30
Ga	30	38	30	30	30	30	30	30	34	30
Sc	20	20	20	23	20	20	20	20	28	20
Cl	628	788	812	225	313	429	823	513	2320	277

The carbon content varies from 5 to 32 wt % and sulfur content range of 2 to 28 wt %. Along with these elements, the rocks also contain volatile components: 225 to 2320 ppm Cl, and 0.01to 0.6 wt % P2O5, a

fact suggesting the action of transport reactions. The percentage of silica is variable high to low in some samples of rang between 12 to 51 wt %. SiO_2 shows negative or inverse relationship with Fe_2O_3, MgO, TiO_2, K_2O, S, C and LOI whereas positive correlation with Al_2O_3, Na_2O, CaO and P_2O_5 (Fig. 19). The percentage of Al_2O_3 is in excess with range of 5 to 20 wt %., it's found in biotite, feldspar and plagioclases. Na_2O and K_2O display variable or inverse relationship but relatively high concentrations ranging from 0.2 to5 wt% and 1.5 to 5 wt% respectively (Fig. 20a). Na_2O and K_2O indicate the presence of sodic feldspar (albite) and K- feldspar respectively. The MgO contents of studied samples are correlated with K_2O contents (Fig. 20b), indicating presence of a magnesium-bearing (chlorite, biotite) and muscovite.

The studied rocks show high content of Fe_2O_3 in most samples ranging from 5 to 60 wt %. The Fe oxides contents show positive relation with S content (sulphur) seems to suggest that Fe is mainly associated with sulfide minerals such as pyrite and pyrrhotite (Fig. 20c). The positive relation coefficient between CaO and P_2O_5 suggest that Ca is mainly associated with apatite (Fig. 20d). Other oxides as TiO_2 and MnO are present at low contents.

The studied graphite schist samples show, however, remarkably large variation in graphitic C concentrations varying from 5 to 32 wt%. The highest C content occur at sample R315 (43.50-43.55) while at sample R307 (22.0-22.05) graphitic C remains in much lower levels. Sulphur contents of the studied graphite-rich black schist range of 2 to 28 wt%. Practically all sulphur is distributed in iron sulphides (pyrite and pyrrhotite) because of the fact that other sulphides are rare and occur only sporadically. In the graphite-bearing biotite schist deposits investigated in this study, there is generally strong or good positive correlation of graphitic carbon with loss of ignition and SiO_2 (Fig. 21a, b). However, C correlates negatively against Fe_2O_3 and sulfur (Fig. 21c, d).

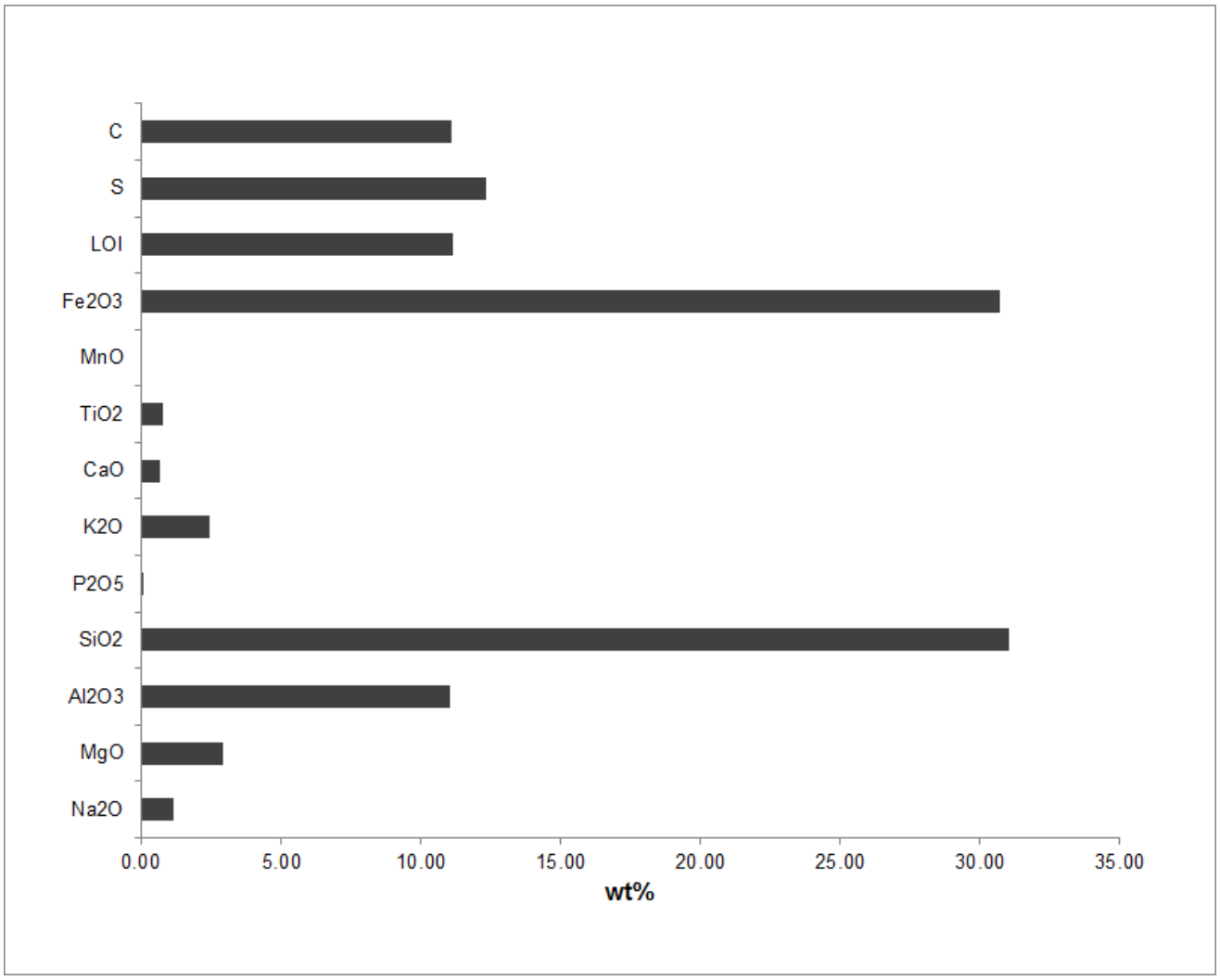

Figure 19. *Distribution graph of major oxides, sulfur and carbon in the studied rock samples.*

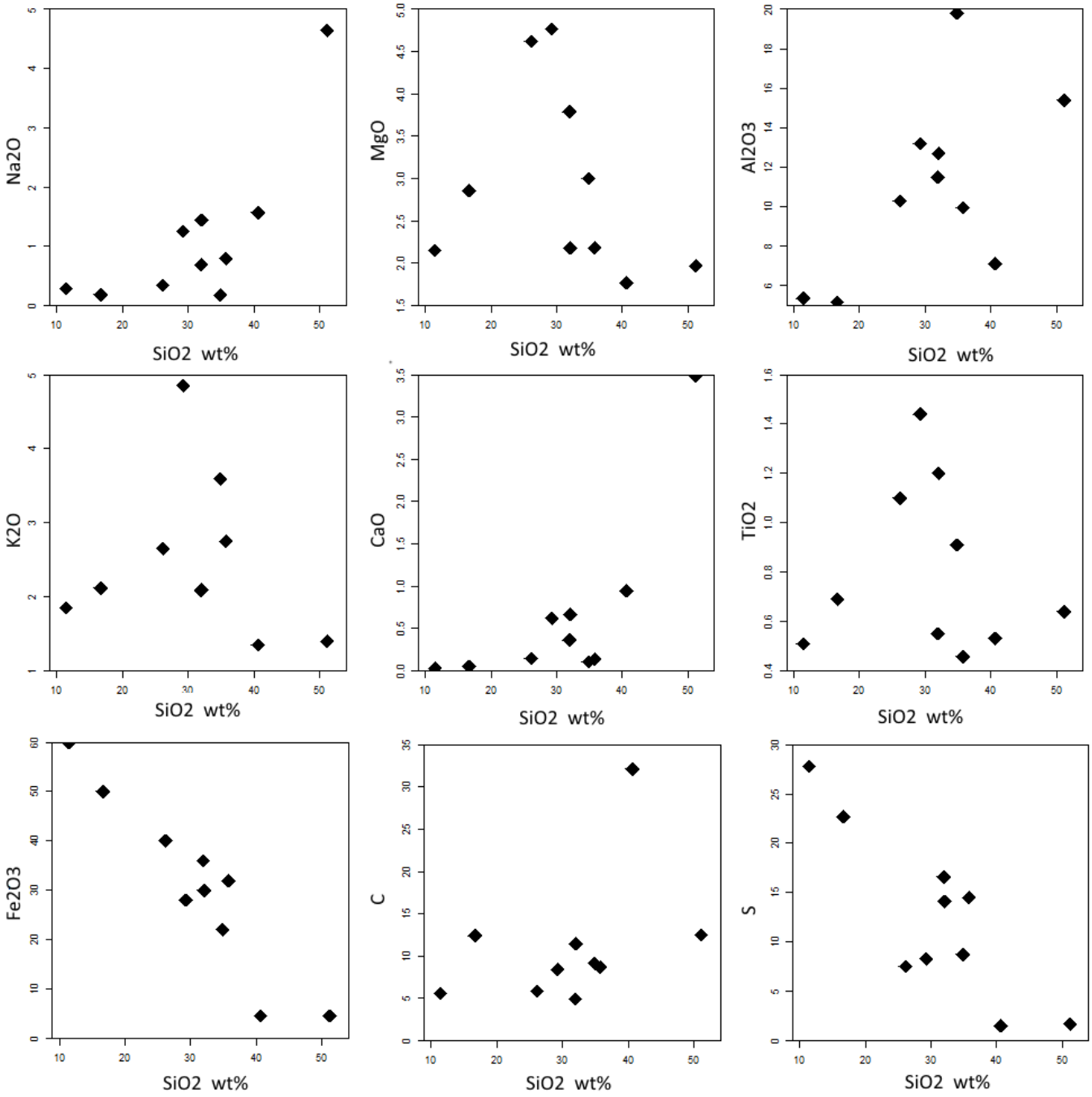

Figure 20. *Hacker diagrams shows major element variation with SiO2*

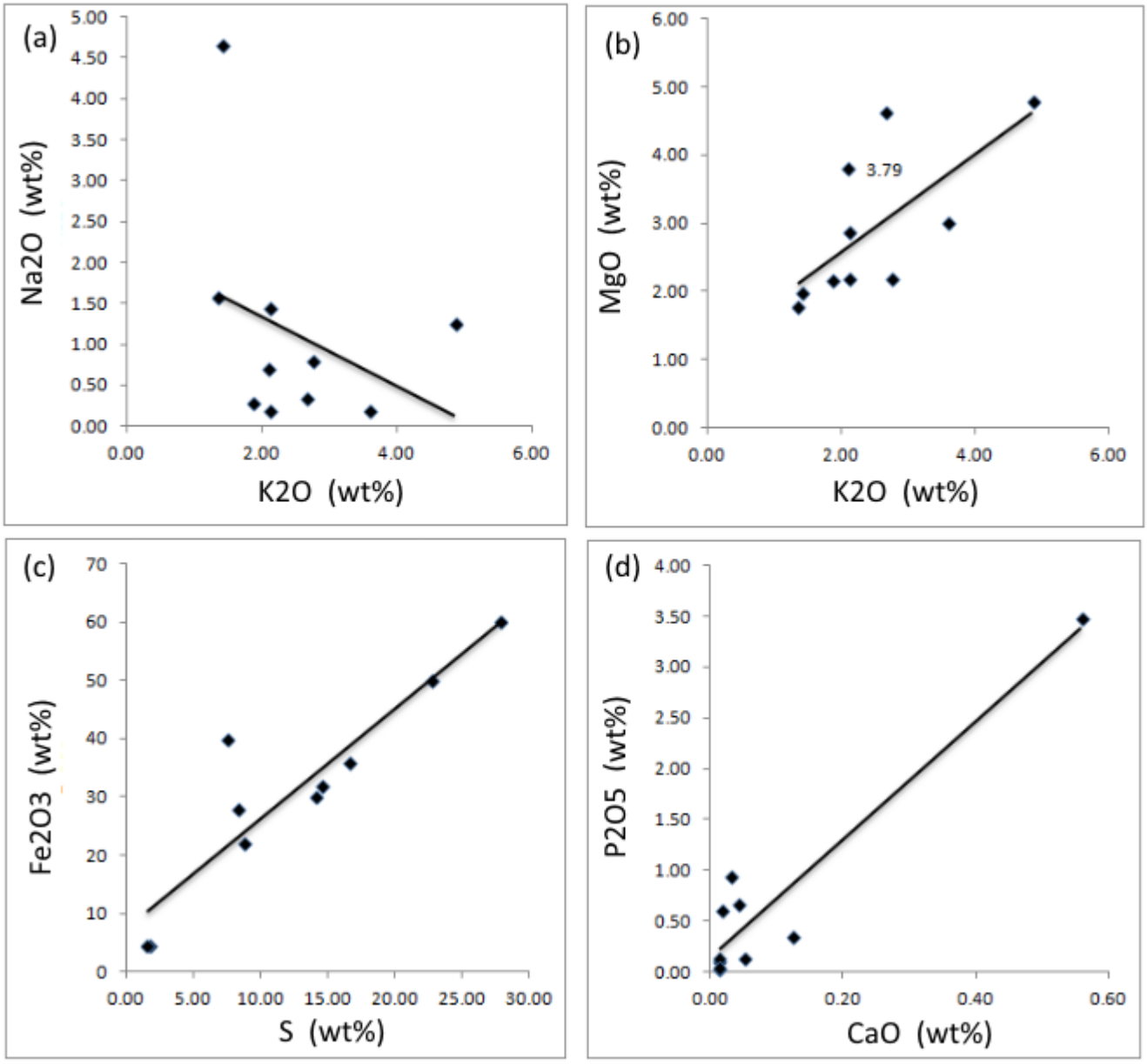

Figure 21. *(a, b) Plot of K2O against Na2O and MgO respectively, (c) Plot Fe2O3 against sulfur, (d) CaO against P2O5 in studied black schists.*

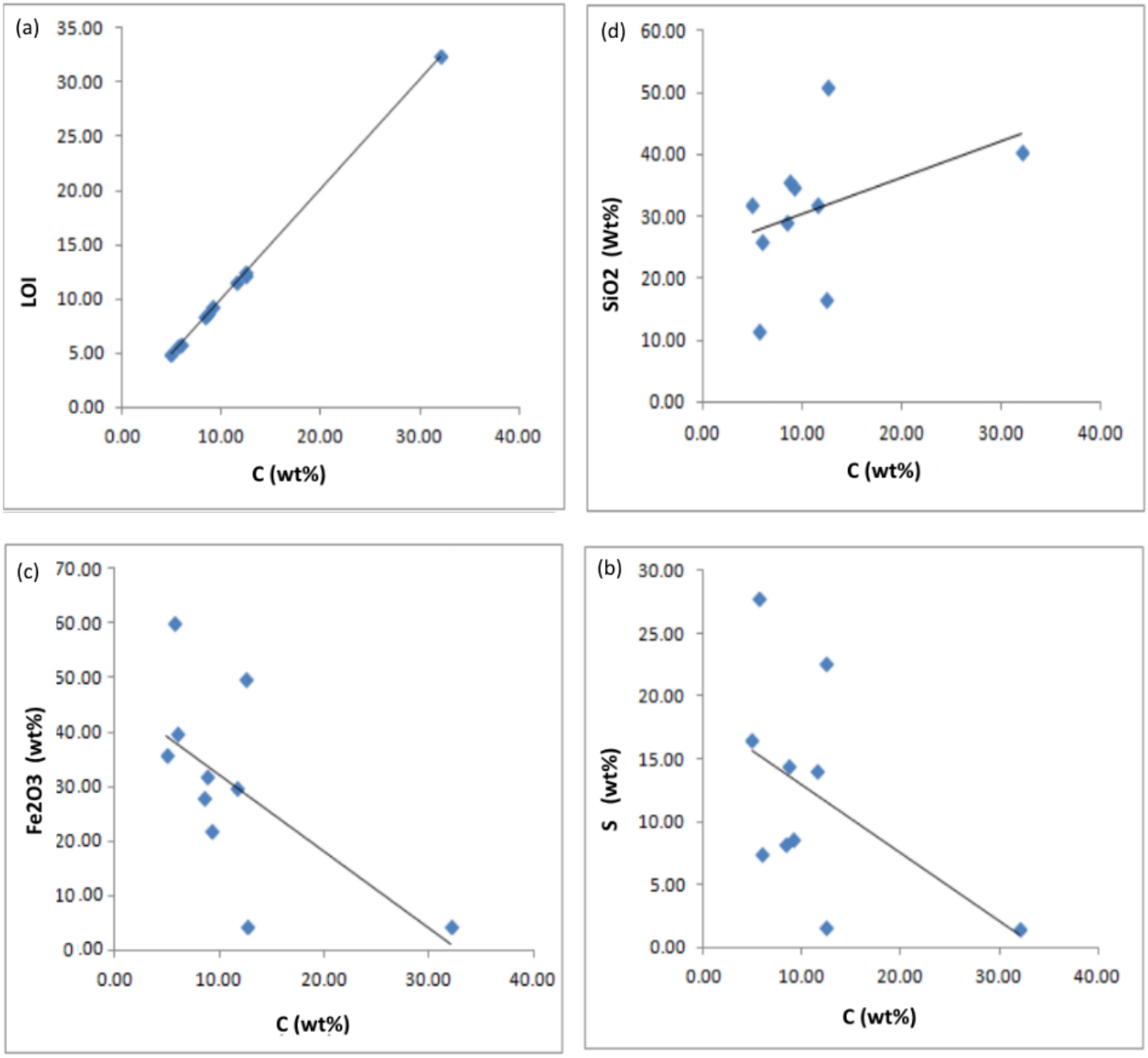

Figure 22. *Plot of graphite against LOI, SiO2, Fe2O3 and sulfure respectively.*

6 DISCUSSION

Graphite deposits result by metamorphism of sedimentary carbonaceous matter or from precipitation of carbon-bearing fluids On the basis of the mineralogy, texture s, structures, metamorphic - fluid conditions, crystallinity of the flake graphite and degree of graphitization of the studied graphite mineralized

areas, a model for the development of the graphite is presented. The transformation of carbonaceous material to fully ordered graphite is dependent on the temperatures during diagenesis and metamorphism (Buseck and Beyssac, 2014). The grade of metamorphism is thus essential for the quality of flake graphite. Therefore micro-graphite flakes (amorphous) are the result of low-grade metamorphism and those having well-developed flakes of graphite (flaky) are due to medium to high grade metamorphism.

Our petrographic and SEM studies have shown how the graphite flakes are evenly distributed in the graphite schist and are up to >1mm in size. The graphite flakes are oriented uniformly along with other flaky minerals to form the schistose structure. The strong foliation of the sample is formed by platy graphite, biotite, and the flat faces of strongly flattened and coarsely sutured quartz. Alternate layers of graphite along with mica flakes and calcareous bands are also noticed. By using XRD we could establish that the studied graphite is well ordered. The calculated graphitization degree suggests a high temperature formation of the graphite of the order of 650°C ± 100°C, which is in agreement with the available geothermometry data for the terrain. The present study extends the idea that the graphite crystallization is always a progressive reconstruction process even to the highest grades of metamorphism and is an irreversible phenomenon, which has the potential to be used as a metamorphic thermometer to assess the peak metamorphic temperature. The genesis of the graphite veins in the studied area is believed to be a consequence of the high grade metamorphism in the presence of a deep-seated crustal CO2-rich fluid phase, whose high pore fluid pressures promoted the development of these veins by hydraulic fracturing under regional syntectonic deformation. The textures and structures of type 1) flake and needle graphite suggest a process of graphite precipitation partly from CO2-rich fluids in hydraulic fractures by a crack - seal fiber growth mechanism (Ramsay and Huber 1983).

7 CONCLUSIONS

The economic potential of a graphite-bearing rock depends mainly on the graphite carbon content and flake size, since the market price for graphite reflects these two characteristics. The thickness of the graphite black schist in the intercalations investigated in Kuusivaara and Joutsijärvi areas usually varies between 2 and 5 m, but may reach 10 m in places, . The studied graphite schists show medium to high median graphite and sulphur concentrations, with the mean values varying between 2% to 28.7% and 5 to 32 %, respectively. Pyrrhotite and pyrite are by far the most common sulphides, whereas chalcopyrite and sphalerite occur sporadically and are totally absent in some samples. However, the graphite grains have their longest axes greater than 100 μm, which suggests that flake size is optimal and that it is technically feasible to produce graphite concentrates using the available technology.

The d (002) values of the graphite crystals and their high crystallite size Lc (002), suggests that the studied graphite is well ordered. The calculated graphitization degree suggests a high temperature formation of the graphite of the order of 650°C ± 100°C, which is in agreement with the available geothermometry data for the terrain. The present study extends the idea that the graphite crystallization is always a progressive reconstruction process even to the highest grades of metamorphism and is an irreversible phenomenon, which has the potential to be used as a metamorphic thermometer to assess the peak metamorphic temperature.

8 REFERENCES

Arkimaa, H., Hyvönen, E., Lerssi, J., Loukola-Ruskeeniemi, K., Vanne, J., 2000. Proterozoic Black Shale and Aeromagnetic Anomalies in Finland. Scale 1: 1 000 000. Geological Survey of Finland, Espoo.

Baiju KR, Satish-Kumar M, Kagi H, Nambiar CG, Ravinsankar M., 2005. Mineralogical characterization of graphite deposits from Thodupuzha-Kanjirappally Belt, Madurai Granulite Block, and Southern India. Gond Res 8: 223-230.

Buseck, P.R. & Beyssac, O. 2014: From Organic Matter to Graphite: Graphitization. Elements 10, 421–426. Doi: 10.2113/gselements.10.6.421.

Ferry. J. M. 1981. Rb-Sr whole-rock and 40K/39Ar mineral ages of the Togus and Hallowell quartz monzonite and Three Mile Pond, Am. Mineral 66:908–30.

Frauenfelder, K.O.H., 1924. Der Graphite in Finland, seiner Entstehung und Verwertung. Geoteknisiä Griffin, G.M., 1967. X-ray diffraction techniques applicable to studies of diagenesis and low rank metamorphism in humid sediments. J. Sediment. Petrol., v. 37, pp. 1006-1011.

Howe, J.Y., Kawn, C.J., Jones, L.E. and Ow, H., 2003. Improved crystallographic data for graphite. Powder diffraction, v. 18, pp. 150.154.

Katz, M.B., m., 1987. Graphite deposits of Sri Lanka: a consequence of granulite facies metamorphism. Mineralium Deposita 22, 18-25.

Landis, C.A., 1971. Graphitization of dispersed carbonaceous material in metamorphic rocks. Contributions to Mineralogy and Petrology 30, 34-35.

Lazzeri M, Barreiro A., 2014. Graphitic carbon: carbon-based nanoscience. Elements 10: 447-452.

McClay, K.R. and Ellis, P.G., 1983. Deformation and recrystallization of pyrite. Mineral. Mag., 47,

52738.

Pankka H., 1999. Exploration report covering the claim area Kuusivaara 1, Mine Reg. N: O 6157/1 and Aapalampi 1-2, Mine Reg. N: O 6158/1 – 2 in the Kemijärvi. GTK Research Report M06/3632, 3634/-99/1/10.

Ramsay, J.G., Huber, M., 1983. The Techniques of Modern Structural Geology. Volume 1: Strain Analysis. Academic Press, London.

Statistic 2015 Major countries in worldwide graphite production 2010-2015, www.statista.com

Tagiri, M., 1981. A measurement of graphitizing-degree by the X-ray powder diffractometer. J. Japan. Asoc. Mineral. Petrol. Econ. Geol., v. 76, pp, 345-352.

Tagiri, M. and Oba, T., 1986. Hydrothermal synthesis of graphite from bituminous coal at 0.5-5.0 kbar water vapor pressure and 300-600°C. J. Japan. Asoc. Mineral. Petrol. Econ. Geol., v. 81, pp. 260-271.

Tagiri, M. and Tsuboi, S., 1979. Mixed carbonaceous material in Mesozoic shales and sandstones from the Yamizo mountain system, Japan. J. Japan. Asoc. Mineral. Petrol. Econ. Geol., V. 74, pp. 47-56.

Tiwary, A., Deb, M. and Cook, N.J., 1998. Use of pyrite microfabric as a key to the tectono-thermal evolution of massive sulphide deposits an example from Deri, Southern Rajasthan, India, Mineralogical Magazine, April 1998, Vol. 62(2), pp. 197–212.

Wada, IH., Tomita, T., Iuchi, K., Ito, M. and Morikiyo, T., 1994. Graphitization of carbonaceous matter during metamorphism with reference to carbonate and pelitic rocks of contact and regional metamorphism, Japan. Contrib. Mineral. Petrol., v. 118, pp. 217-228

U.S. Geological Survey, 2015. Mineral Commodity Summaries, January

APPENDICES

APPENDIX 1. XRD OF GRAPHITE SAMPLES.

GEOLOGICAL SURVEY OF FINLAND RESEARCH REPORT 1 (2)
Mineral processing and material research
EMA-2016-36-X
Mia Tiljander 29.3.2016

Customer: Thair Al-Ani / GTK, project 50402-20048

Reference of the research

Graphite samples from Kuusivaara, Northern Finland. Mineral identification with X-ray diffraction (XRD).

Results

Sample was powdered fine in agate mortar and measured over the range 2-70 °2Θ CuKα with Bruker D8 Discover A25 diffractometer. Adjustments of the generator were 40 kV/40 mA, step size 0.02° and measurement time 0.2 s.

Phases were identified with Bruker's EVA (4.0) software using ICDD (International Centre for Diffraction Data) database PDF-4 Minerals 2014.

Estimation about amorphous content comes directly from EVA program. The amounts of the amorphous material are very likely overestimated. There is no clear background hump in any sample.

The following crystalline phases were identified:

3634-96-R302 31.90 (LabID 201600125):

Graphite, phlogopite, pyrrhotite, cordierite, rutile, quartz and possible kaolinite.

Amorphous material c. 32 %.

3634-96-R305 20.80 (LabID 201600126):

Graphite, pyrrhotite and phlogopite.

Amorphous material c. 35 %.

Geologian tutkimuskeskus | Geologiska forskningscentralen | Geological Survey of Finland
Espoo • Kokkola • Kuopio • Loppi • Outokumpu • Rovaniemi
www.gtk.fi • Puh./Tel. +358 29 503 0000 • Y-tunnus / FO-nummer / Business ID: 0244562-7

3634-96-R314 24.00 (LabID 201600127):

Graphite, plagioclase, quartz, pyrite, phlogopite and possibly apatite.

Amorphous material c. 20 %.

3634-96-R316 46.80 (LabID 201600128):

Graphite, phlogopite, plagioclase and pyrrhotite.

Amorphous material c. 25 %.

3634-96-R314 47.60 (LabID 201600129):

Graphite, phlogopite and pyrrhotite.

Amorphous material c. 20 %.

3634-96-R306 49.15 (LabID 201600130):

Graphite, kaolinite, pyrrhotite, quartz, phlogopite, rutile and chlorite.

Amorphous material c. 25 %.

3634-96-R320 22.90 (LabID 201600131):

Graphite, pyrrhotite, quartz, phlogopite, plagioclase, K-feldspar and possibly kaolinite.

Amorphous material c. 35 %.